Continental Shelf Research 138 (2017) 1–18

Contents lists available at ScienceDirect

Continental Shelf Research

journal homepage: www.elsevier.com/locate/csr

Research papers

Inner-shelf ocean dynamics and seafloor morphologic changes during Hurricane Sandy

John C. Warner[a,*], William C. Schwab[a], Jeffrey H. List[a], Ilgar Safak[a], Maria Liste[b], Wayne Baldwin[a]

[a] Coastal and Marine Geology Program, US Geological Survey, 384 Woods Hole Road, Woods Hole, MA 02543, USA
[b] Integrated Statistics, Woods Hole, MA, USA[1]

ARTICLE INFO

Keywords:
Shoreface connected sand ridges, sediment transport
Fire Island, NY
Hurricane Sandy
Inner shelf
Numerical modeling

ABSTRACT

Hurricane Sandy was one of the most destructive hurricanes in US history, making landfall on the New Jersey coast on October 30, 2012. Storm impacts included several barrier island breaches, massive coastal erosion, and flooding. While changes to the subaerial landscape are relatively easily observed, storm-induced changes to the adjacent shoreface and inner continental shelf are more difficult to evaluate. These regions provide a framework for the coastal zone, are important for navigation, aggregate resources, marine ecosystems, and coastal evolution. Here we provide unprecedented perspective regarding regional inner continental shelf sediment dynamics based on both observations and numerical modeling over time scales associated with these types of large storm events. Oceanographic conditions and seafloor morphologic changes are evaluated using both a coupled atmospheric-ocean-wave-sediment numerical modeling system that covered spatial scales ranging from the entire US east coast (1000 s of km) to local domains (10 s of km). Additionally, the modeled response for the region offshore of Fire Island, NY was compared to observational analysis from a series of geologic surveys from that location. The geologic investigations conducted in 2011 and 2014 revealed lateral movement of sedimentary structures of distances up to 450 m and in water depths up to 30 m, and vertical changes in sediment thickness greater than 1 m in some locations. The modeling investigations utilize a system with grid refinement designed to simulate oceanographic conditions with progressively increasing resolutions for the entire US East Coast (5-km grid), the New York Bight (700-m grid), and offshore of Fire Island, NY (100-m grid), allowing larger scale dynamics to drive smaller scale coastal changes. Model results in the New York Bight identify maximum storm surge of up to 3 m, surface currents on the order of 2 ms^{-1} along the New Jersey coast, waves up to 8 m in height, and bottom stresses exceeding 10 Pa. Flow down the Hudson Shelf Valley is shown to result in convergent sediment transport and deposition along its axis. Modeled sediment redistribution along Fire Island showed erosion across the crests of inner shelf sand ridges and sedimentation in adjacent troughs, consistent with the geologic observations.

1. Introduction

Recent extreme storm impacts on the US East Coast include Hurricane Isabel in 2003, the extratropical system Nor'Ida in 2009, Hurricane Irene in 2011, and Hurricane Sandy in 2012, one of the most costly and destructive storms in US history. Hurricane Sandy developed into a tropical storm in the Caribbean Sea on October 22, 2012, and intensified into a hurricane on October 24 as it traveled north across the Caribbean Islands. The storm evolved through several cycles of intensity as it traveled along the US East Coast and eventually reached a Category 2 with winds exceeding 154 km/h (96 mi/h) on October 29 well offshore of Cape Hatteras, NC. The storm then weakened to a post tropical cyclone before making landfall near Brigantine, New Jersey, on October 29 at 2300 UTC with winds on the order of 70 km/h (44 mi/h) (Blake et al., 2013; Fig. 1).

Assessment of the impact of Hurricane Sandy identified damage from winds, flooding from rainfall and storm surge, and coastal erosion. The alterations to the coast included massive redistribution of sediment in the coastal zone, reduction of dune heights, and several barrier island breaches (e.g., Hapke et al., 2013; Sopkin et al., 2014).

* Corresponding author.
E-mail addresses: jcwarner@usgs.gov (J.C. Warner), bschwab@usgs.gov (W.C. Schwab), jlist@usgs.gov (J.H. List), isafak@usgs.gov (I. Safak), mlistemunoz@usgs.gov (M. Liste), wbaldwin@usgs.gov (W. Baldwin).
[1] Under contract to US Geological Survey

http://dx.doi.org/10.1016/j.csr.2017.02.003
Received 2 April 2016; Received in revised form 1 February 2017; Accepted 6 February 2017
Available online 17 February 2017
0278-4343/ Published by Elsevier Ltd.

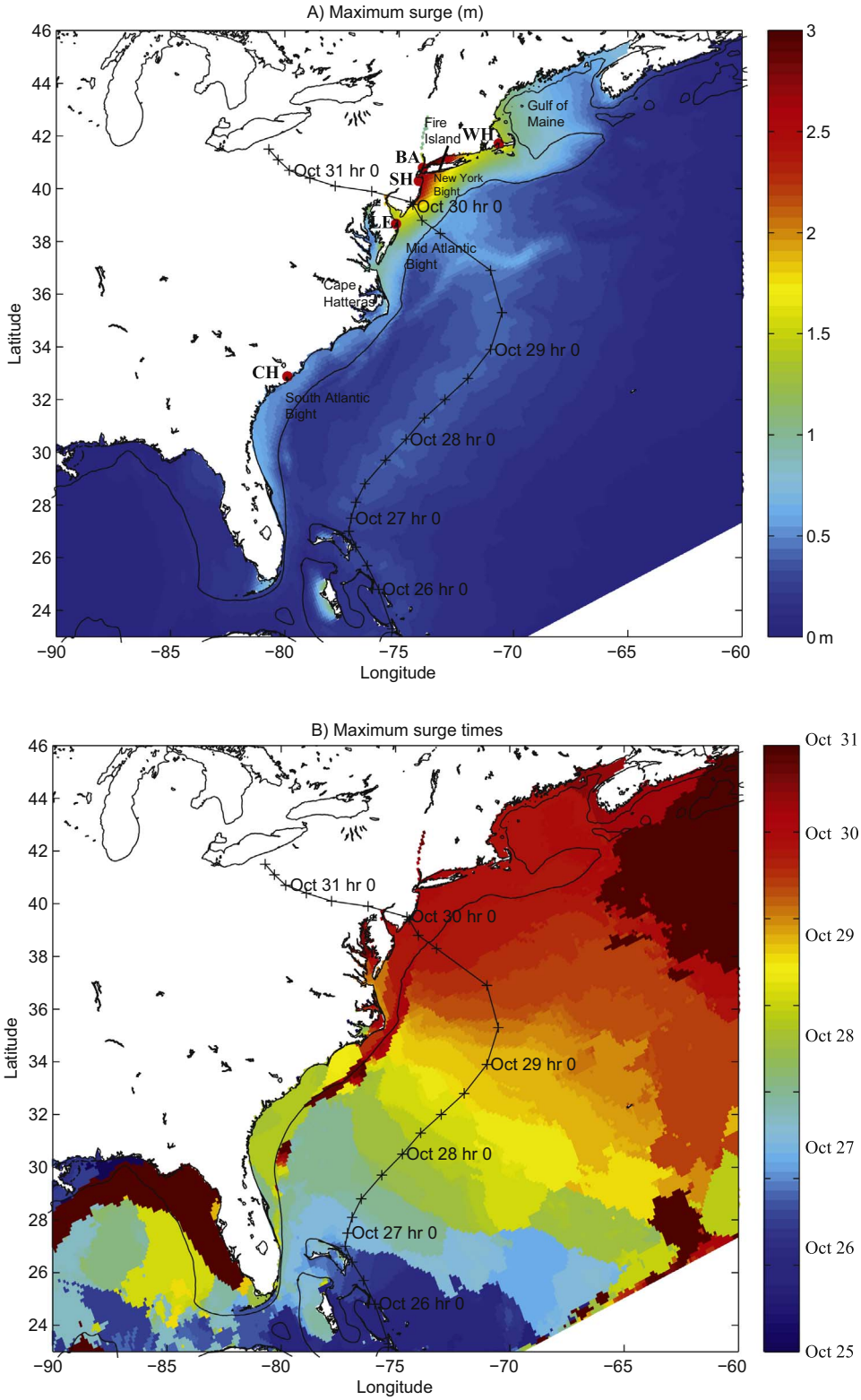

Fig. 1. Map of US East Coast showing track of Hurricane Sandy (black line with –x- and timed positions), 100 m isobaths (thin black line), and numerical results of (A) maximum water level surge (increase of water level above normal tide) and (B) timing of maximum surge. Locations shown in (A) for water level stations of Fig. 5 (WH: Woods Hole; BA: Battery; SH: Sandy Hook; LE: Lewes; and CH: Charleston).

These changes to the subaerial component of the coastal system can be evaluated, both over the long-term and in response to severe storms, through the use of repetitive aerial photographs and airborne lidar topographic surveys. However, changes to the adjacent subaqueous regions, including the shoreface and inner continental shelf, are not as easily assessed, even though they compose the fundamental framework of the coastal zone, and are critical areas with regard to navigation, aggregate resources, marine habitats, and seafloor morphological evolution. The thickness and distribution of mobile sediments on the inner continental shelf is poorly documented in most areas, and little is known about how these sedimentary deposits are modified during high-energy events such as extratropical storms and hurricanes.

Understanding the form and magnitude of seafloor morphologic change is critical to developing coastal sediment budgets, as well as increasing our knowledge of how these processes are time-integrated into the decadal and longer timescales of continental margin sedimentation (e.g., Riggs et al., 1995; Schwab et al., 2013; Miselis and McNinch, 2006; Denny et al., 2013).

Observations of impacts to the seafloor in the coastal zone (including shoreface and inner continental shelf) from hurricanes are sparse due to the logistical and technological difficulty in data collection required for measuring seafloor changes (e.g., Goff et al., 2015; Schwab et al., 2016). Observations of oceanographic and sediment transport conditions during hurricanes are also typically rare, and often observed by chance (Wren and Leonard, 2005; Teague et al., 2007). However, these types of observations are becoming more available as long-term instrumented ocean observatories are sustained and new techniques using remote vehicles allow observations during the events (e.g., Miles et al., 2015).

As compared to observations, numerical simulations of hurricanes and severe Nor'Easters are more readily available. Predictions have shown substantial improvements over the past few decades primarily though improvements to coarse-grid, global models (Goerss, 2006; Marks and Shay, 1998; Wang and Wu, 2004; Bender et al., 2007). Forecasts of hurricane tracks have shown gradual improvements over the years, primarily attributed to several research areas including improved assimilation of satellite and aircraft observations, better representation of the hurricane vortex, and improved representation of tropical physics (Rogers et al., 2006). However, improvement in tropical cyclone intensity prediction has been slower to develop (Rogers et al., 2006; Wada et al., 2010), often attributed to deficiencies of numerical models in three areas: coarse grid spacing, poor formulations of the surface and boundary layers, and lack of coupling to a dynamic ocean (Chen et al., 2007).

Developments of coupled modeling systems have progressed recently, with a full review of recent advances and core technical and scientific issues summarized by Peng et al. (2012). A main advantage of coupling an ocean, sea ice, or wave model to an atmosphere model is that they provide the atmosphere with dynamic feedbacks of sea surface temperatures and surface roughness for momentum and heat flux computations. These in turn modify the atmospheric processes and feedback to the ocean and wave dynamics. Model coupling has been shown: 1) to increase predictability of sea surface temperatures for simulating Hurricane Isabel (2003; Warner et al., 2010); 2) the effects of waves to increase the sea surface roughness thus creating reduced wind speeds and producing more accurate atmosphere - ocean dynamic during Nor'Ida (2009; Olabarrieta et al., 2012); 3) to provide more accurate intensity predictions for Hurricane Ivan due to sea surface temperature feedbacks (2004; Zambon et al., 2014a); 4) that there was a lack of significant ocean feedback on the hurricane intensity dynamics for Hurricane Sandy because of its fast translation speed (2012; Zambon et al., 2014b); and 5) the significance of air-sea exchanges during extratropical cyclones (Nelson et al., 2014) and coastal storm events (Renault et al., 2012).

Although numerical simulations of large-scale storm events have advanced in recent years, predictions of sediment transport and geomorphic change are still challenging. A common agreement is the need to use coupled modeling systems that can communicate dynamic changes between all components of the modeling system during the simulation, such as breaching of barrier islands and wave-current interactions at tidal inlets. These processes can modify water exchange between the open-ocean to back-barrier bays to enhance flooding hazards, and can exchange sediment between the nearshore and inner continental shelf (Olabarrieta et al., 2011; De Vet et al., 2014). Additionally these modeling scenarios require oceanographic observations (waves, winds, currents) to provide ground truth of model predictions and require geologic information to provide baseline data for the composition of the bottom substrate, sediment grain size, seabed roughness, sediment availability, and coastal ocean topography.

In response to Hurricane Sandy, the U.S. Geological Survey (USGS) is leading a multi-faceted mapping and research program designed to guide recovery and restoration efforts (Buxton et al., 2013). Components of the program link coastal processes to vulnerability, including how to quantify offshore sand resources suitable for recovery efforts, establish linkages between nearshore geology, ocean processes, and barrier island response; and develop models that predict the coastal response to oceanographic forcing, assess vulnerability, and predict barrier island evolution. Fire Island, NY, a barrier island along southern Long Island (Fig. 1), and the adjacent inner continental shelf has been a primary focus of the USGS Hurricane Sandy response (http://woodshole.er.usgs.gov/project-pages/coastal_change/study-sites/fire-island.html). The USGS has long been involved in research in the New York inner-continental shelf starting in 1996 with the objectives of evaluating the influence of the regional geologic framework on coastal evolution, and formulating a conceptual model of sediment flux in the coastal ocean (Schwab et al., 2000a, 2013). In May of 2011, the USGS conducted a high-resolution marine geophysical survey of the lower shoreface and inner continental shelf offshore of Fire Island using interferometric sonar and seismic-reflection techniques (Schwab et al., 2014b). Ultimately, this survey served to document conditions on the Fire Island inner continental shelf prior to the passage of Hurricanes Irene (Aug. 2011) and Sandy (Oct. 2012). The USGS, in cooperation with the U.S. Army Corps of Engineers (USACE), conducted additional surveys in 2014 to document post-storm conditions. These additional efforts re-surveyed the 2011 study area using a high-resolution multibeam echosounder, and focused on a series of shoreface-attached sand ridges offshore of western Fire Island using a high-resolution seismic-reflection profiler (Schwab et al., 2016). The objectives of the post-storm surveys were to determine the impact primarily from Hurricane Sandy on the inner continental shelf morphology and modern sediment distribution, and broaden the baseline geospatial framework for sediment transport and coastal change model development. It is further emphasized that the surveys in 2014 included impacts from all events between 2011–2014, however, the impact from Hurricane Sandy is considered the most significant because it had a greater intensity and subaerial impact than any other event in the time period. Additionally, as described in the modeling section, analysis of a forecast modeling archive show the impacts of Irene were significantly less than that of Hurricane Sandy, and further supports that Hurricane Sandy was likely to be the dominant impact during this time period.

The research presented here is part of this larger effort to better understand the physical processes controlling coastal change during large storm events and to further the understanding of storm-driven sediment flux on the inner continental shelf. In this manuscript we focus on the applications of a coupled three-dimensional deterministic numerical modeling system to simulate the oceanographic and morphologic changes during Hurricane Sandy. Because the storm event occurred for many days and covered a large geographic region, the modeling approach encompassed the entire US East Coast and utilized a grid nesting method to provide a refined solution in a region of detailed seafloor observations. Numerical results of oceanographic conditions are compared to observations along the entire US East Coast, and numerical results of morphologic change are also shown for the entire US East Coast with a detailed comparison to observations of geologic framework changes along Fire Island, NY.

2. Geologic setting

The US East Coast is an open coastline that can be broadly characterized by the rocky coast of the Gulf of Maine (GoM) and sandy shores lined with barrier islands predominately in the Mid Atlantic Bight (MAB) and South Atlantic Bight (SAB) (Fig. 1). The continental shelf along the coast varies in width from 5 to 120 km in the SAB from

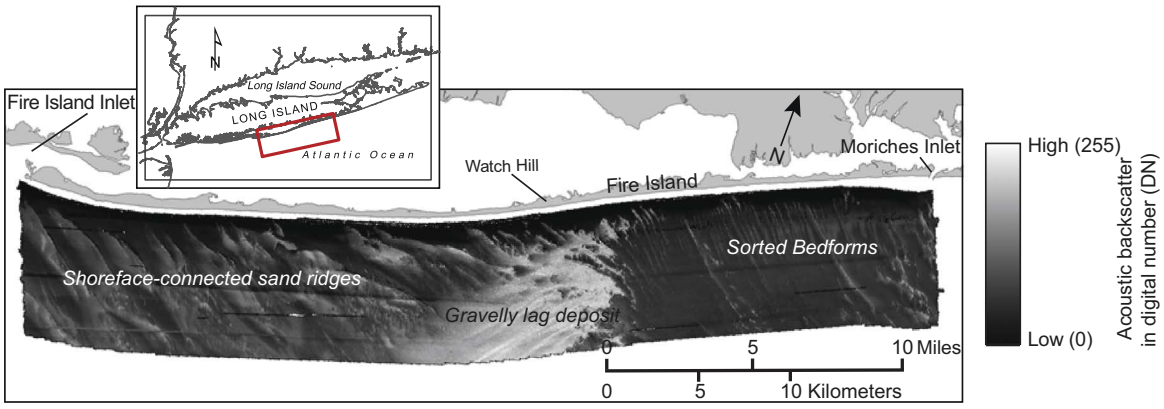

Fig. 2. Site map insert identifies location of principal study area offshore of Fire Island, NY. Map shows backscatter intensity revealing gravelly lag deposit suggested to represent seaward extent of an outwash lobe that liberated sediment to form shoreface connected ridges along western end of Fire Island. Eastern end is comprised of sorted bedforms extending offshore across study region. (Figure modified from Schwab et al., 2016).

100 to 200 km width in the MAB(Fig. 1). Sediment distribution varies locally, but is typically composed of coarse sand, sand, and regions of silt and clay in the SAB and MAB, with increasing content of sandy clay and silty clay in the central region of the GoM (Poppe et al., 2014).

A principal area for our Hurricane Sandy impact study has been the inner continental shelf and southern coastal region along Long Island, NY. Investigations provided a unique geologic framework assessment and inner-shelf changes from an extreme storm event on a regional scale. This region consists of reworked glacial outwash associated with the Wisconsinan Laurentide glacial advance (Stone and Borns, 1986) and includes shallow back-barrier bays, marshes, and low relief, sandy barrier islands (Leatherman, 1985). Located within this barrier-island system is Fire Island, a 0.5-km-wide, 50-km-long barrier island bound by two tidal inlets managed as navigation channels, Moriches Inlet to the east and Fire Island Inlet to the west (Fig. 2). A more thorough review of the regional geologic framework and coastal evolution of the Fire Island study area, including major inner continental shelf sedimentary sequences, sediment distribution, and shelf morphology, is presented in Schwab et al., (2000a, 2013, 2014b), and briefly summarized below.

The inner-shelf offshore of Fire Island is characterized by a centrally located high-backscatter gravelly sand deposit, a series of shoreface connected sand ridges to the west, and a region of sorted bedforms to the east (Fig. 2). East of Watch Hill, the Pleistocene-age outwash deposit, primarily composed of poorly to very poorly sorted, medium-grained sand to gravel, is exposed at the seafloor (Schwab et al., 2013). Here, geophysical data show numerous high-backscatter, < 2 m deep depressions oriented ~60–70° to the shoreline that are interpreted to be sorted bedforms (Fig. 2). Schwab et al. (2013) interpreted the relatively high-backscatter base and eastward-facing flanks of the sorted bedform troughs to be indicative of continued erosion of the seabed by oceanographic processes and net westward transport direction of reworked sediment. In the central part of the region in water depths greater than ~18 m, the eroded remnants of an outwash lobe are identified as a high-backscatter gravelly lag deposit (Fig. 2; Schwab et al., 2014b). Schwab et al. (2013) inferred that erosion of this headland during Holocene marine transgression yielded an abundant volume of very fine- to medium-grained sand, a primary source of sediment for the development of the shoreface-connected sand ridges offshore of western Fire Island.

Shoreface-connected sand ridges (SFCRs), similar to those located offshore of western Fire Island have been described in numerous investigations of the North American inner continental shelf where they have seafloor expressions ranging from ~1–10 m, become more asymmetric with increasing water depth, and their longitudinal axes are typically oriented ~10–50° relative to the shoreline, matching the predominant storm wave approach direction and open into the flow direction of the dominant alongshore current (Duane et al., 1972; McKinney et al., 1974; Swift and Freeland, 1978; Figueiredo et al., 1981; Swift and Field, 1981; Stubblefield et al., 1984). The similarity in characteristics suggests a common set of processes is responsible for the origin and maintenance of these sedimentary structures (Trowbridge, 1995; Falques et al., 1998; Calvete et al., 2001; Nnafie et al., 2014; Warner et al., 2014). These SFCRs offshore of Fire Island vary in size and configuration but are, in general, on the order of 10 km in length, have a crest to trough relief on the order of 6 m, spaced about 3 km apart, and oriented obliquely from the coastline on average about 30 degrees clockwise (Fig. 3). Comparison of the sand ridge morphology with the morphology of the underlying Holocene marine transgressive surface (stratigraphic unconformity separating the modern sand deposit from the underlying Pleistocene deposit; a time-transgressive erosional surface formed by rising sea level) and backscatter variations over the ridges were interpreted to indicate that these ridges have moved westward since formation (Schwab et al., 2014b).

Pre- and post-Hurricane Sandy maps of modern sediment thickness on the inner continental shelf offshore of Fire Island were determined by comparing isopachs produced from interpretations of the 2011 and 2014 seismic-reflection data (Fig. 3B and C). Sediment thicknesses were computed by converting along-track, two-way travel times between the seafloor and the Holocene transgressive unconformity horizon to a thickness, assuming an internal seismic velocity of 1500 m/s (Schwab et al., 2014a). In general, the isopachs of modern sediment vary from a thin veneer to almost 6 m thick to comprise the morphology of the SFCR. There is also a relatively thick modern sediment deposit close to the coast near the western limit of the study area (Fig. 3B). This deposit is the lower shoreface; i.e., the toe of the modern beach platform (Schwab et al., 2013, 2014b).

3. Numerical modeling

To investigate the storm dynamic processes we utilize the COAWST numerical modeling system that incorporates ocean circulation, surface waves, and sediment transport components (Warner et al., 2010). Other capabilities, including an atmospheric model, are available in this coupled system and have been used to investigate Hurricane Sandy atmosphere - ocean dynamics (Zambon et al., 2014a, 2014b). This series of applications, however, utilized a set of atmospheric surface forcings (described below) and ran the other model components to focus on the oceanographic and wave response during the storm. For the oceanographic circulation we use the Regional Ocean Modeling System (ROMS), a three-dimensional, free-surface, topography-following numerical model, which solves finite difference approximations of Reynolds Averaged Navier Stokes (RANS) equations using hydrostatic and Boussinesq approximations with a split-explicit time stepping

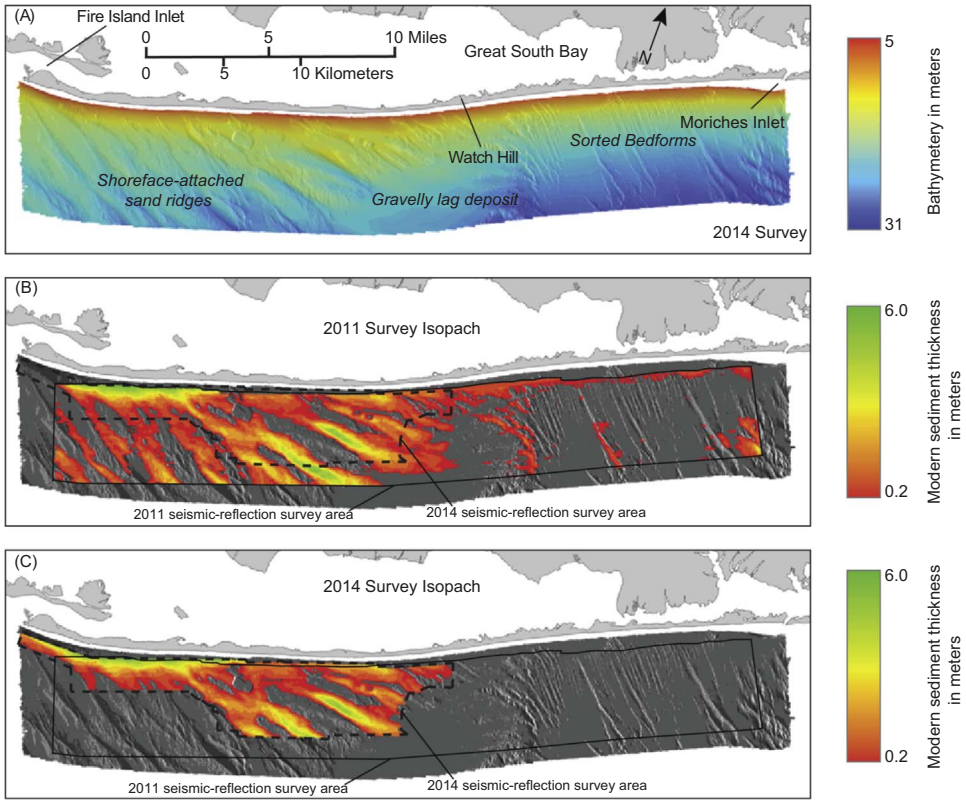

Fig. 3. Map (A) shows the interpolated bathymetric surface generated from multibeam echosounder data collected offshore of Fire Island, NY, in January 2014 (Schwab, et al., 2016). Bathymetry is in meters (m) below the North Atlantic Vertical Datum of 1988 (NAVD 88). Maps (B) and (C) illustrate isopachs of modern sediment thickness derived from seismic-reflection data collected in 2011 and 2014, respectively. These isopachs are overlain on the sun-illuminated bathymetric surface shown in Map (A). West of Watch Hill the modern sand deposit is organized into a series of shoreface-attached sand ridges oriented obliquely to the shoreline. The Pleistocene glacial outwash units from which the modern sands were reworked are exposed in the troughs between the ridges and across other portions of the inner shelf where the modern deposit is absent. The presence of sorted bedforms on the inner continental shelf east of Watch Hill is indicative of this active erosion of the glacial outwash units (Schwab et al., 2014a, 2014b). Figure modified from Schwab et al (2014a).

algorithm (Shchepetkin and McWilliams, 2005; Haidvogel et al., 2008; Shchepetkin and McWilliams, 2009). ROMS includes options for various model components such as different advection schemes (second, third and fourth order), turbulence closure models (e.g., Generic Length Scale mixing, Mellor-Yamada, Brunt-Väisälä frequency mixing, user provided analytical expressions, K-profile parameterization), and several options for boundary conditions. For surface waves, the model utilizes the Simulating Waves Nearshore (SWAN), a spectral wave model that solves for the transport of wave action density and includes source terms from wind and sink terms to include wave energy dissipation due to whitecapping, breaking, and bottom friction (Booij et al., 1999). The sediment routines are from the USGS Community Model for Coastal Sediment Transport (Warner et al., 2008) and include many capabilities such as suspended load, bed load, cohesive and non-cohesive, and multiple sediment classes. This specific application only used the non-cohesive routines for suspended and bedload transport.

The numerical simulations were performed on a coupled, triple-nested grid configuration. The outermost grid covers the US East Coast and Gulf of Mexico with a spatial resolution on the order of 5 km (Fig. 4A). This US East grid (USE) is typically large enough to encompass the full scale of a hurricane or extra-tropical storm system. Nested within the USE grid by a scale factor of 7 is the New York Bight grid (NYB) with a spatial resolution on the order of 700 m (Fig. 4B). This scale was selected to capture the landfall of Hurricane Sandy. The third grid was further nested with a scale factor of 7 to cover the inner continental shelf (SHF) within the extent of Fire Island study area (Fig. 4C) and has a spatial resolution on the order of 100 m. All three grids were simulated concurrently as a nested-coupled application: two-way ocean refinement and one-way wave refinement with fully coupled exchanges between all three grids for the fields of water levels, currents, bathymetry, and bottom roughness from the ocean to the wave model; and wave dissipation, height, length, direction, surface and bottom periods, and bottom orbital velocities from the wave to the ocean model. The relevant ocean physics that include waves are surface enhanced roughness due to the waves from Taylor and Yelland (2001), surface enhanced flux of turbulent kinetic energy due to wave breaking based on Craig and Banner (1994) with an increased roughness dependent on the sea state (Carniel et al., 2009), wave effects on currents as described in Kumar et al. (2012) based on the approach from Uchiyama et al. (2010), and the enhanced bottom roughness due to waves from Madsen (1994). The wave dynamics that are enhanced from coupling to the ocean model include the effects of varying bottom roughness, changes in water level, and effects from near-surface currents based on Kirby and Chen (1989).

The larger USE grid is run as part of a coupled daily forecast that has been ongoing for the past several years (Warner et al., 2010). For the numerical simulations as part of this specific study, the initial conditions for all 3 grids were obtained from that forecast database, and then the triple nested configuration was simulated from October 25 to November 5, 2012. This encompasses the period from when the hurricane first began to impact the southern coast of the US, until after it made landfall. Model results from the forecast on the larger grid will also be presented on days before and after the triple nested configuration to show continuity of output.

For the triple nested configuration, the ocean model was forced with atmospheric data of winds, pressure, air temperature, relative humidity, precipitation, and heat fluxes from combined data sets of NAM and NARR (http://nomads.ncdc.noaa.gov/data.php). Lateral open boundaries were prescribed with velocity, salt, and temperature

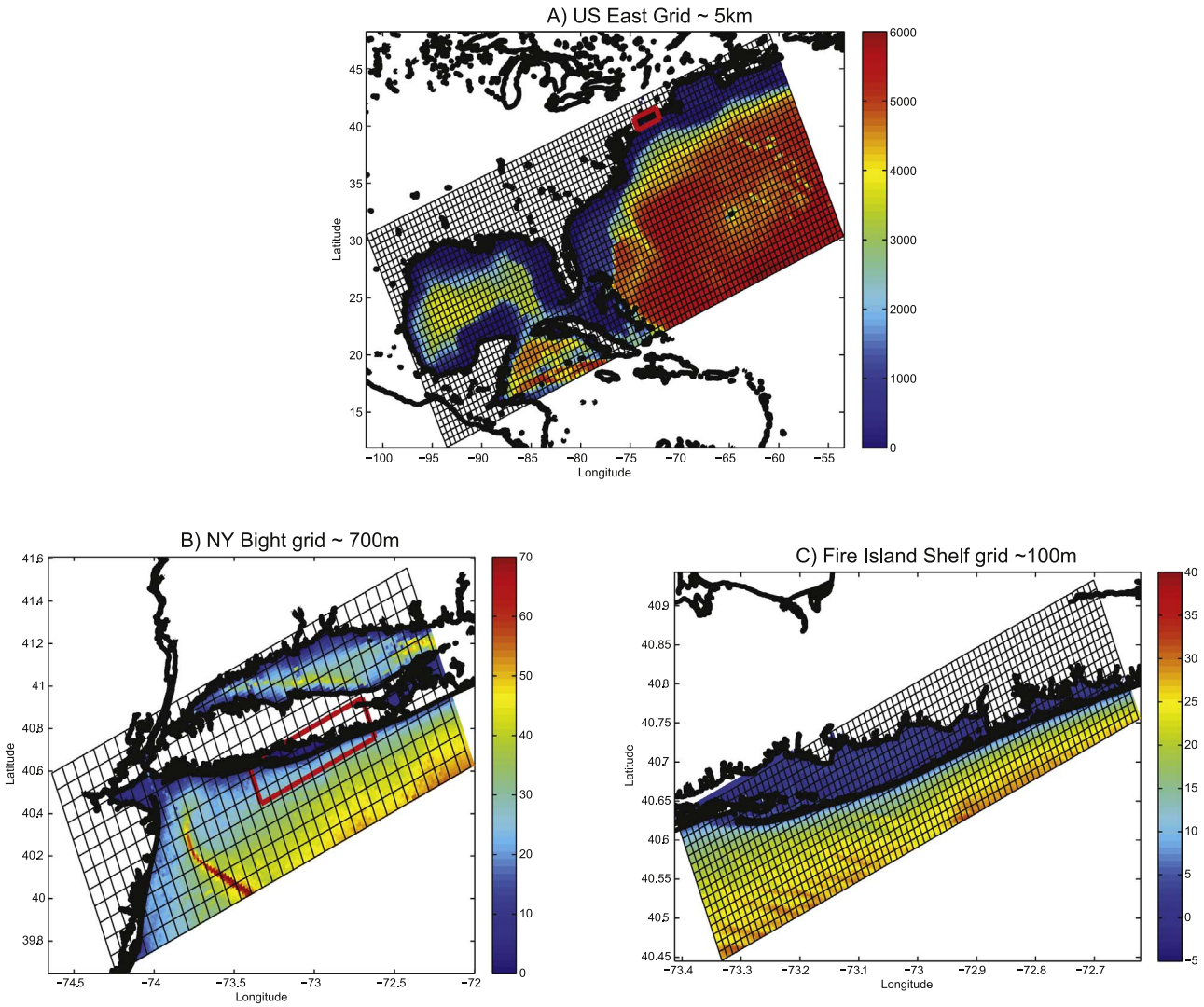

Fig. 4. Numerical model grids for both ROMS and SWAN configured for refined concurrent coupling. Every 10th grid line shown for clarity, with grid resolution approximately: A) USE, 5 km; B) NYB, 700 m; and C) SHF, 100 m.

from HYCOM (http://tds.hycom.org/thredds/dodsC/GLBa0.08/expt_90.9), and during the simulation the model tracer fields of salinity and temperature were nudged to HYCOM data on a four-day time scale. The wave model was simulated with the same wind forcing as the ocean and was also prescribed with parametric wave data along the USE grid open boundary from WaveWatch III (ftp://polar.ncep.noaa.gov/pub/history/waves/). In practicality, due to the magnitude of this storm and the extent of the USE grid, the lateral wave boundaries did not have significant influence on the model results.

For the USE grid, the sediment texture was initialized from the USGS national sediment database (Poppe et al., 2014) and includes six grain-size classes that are described in Table 1 (with parameter values used for Equation 23, Warner et al., 2008). This distribution has been numerically evolving for the past several years as part of a forecast system and results presented here include that evolution. The NYB and SHF grids were also initialized with the same six classes. These classes represent the range of material observed on the seafloor in this region (Schwab et al., 2000b). However, because adequately resolved spatial distributions are not available for all regions of these refined grids, they were initialized with a uniform sediment distribution composed of the same six classes. Sensitivity tests were performed to evaluate initial sediment distributions and sensitivity to erosion rate magnitudes. Results indicate that spatial patterns remained consistent and were not sensitive to the initial sediment field. However the magnitude of bed elevation change did depend on initial conditions, the number of grain size classes used, and more significantly to erosion rate parameters. These values were based on comparisons to other modeling scenarios and local (non-hurricane) storm observations. Ultimately, the spatial patterns remained the same, only the magnitude of change varied.

Table 1
Modeled sediment types.

Mean grain size (phi) (mm)	Density (kg m^{-3})	Settling velocity (mm s^{-1})	Erosion rate (kg m^{-2} s^{-1})	Critical erosion stress (Pa)	Bed porosity (-)
(0) 1.0	2650	140.0	1E-3	0.53	0.7
(1) 0.5	2650	57.0	1E-3	0.27	0.7
(2) 0.25	2650	27.0	1E-3	0.19	0.7
(3) 0.125	2650	8.7	1E-3	0.14	0.7
(4) 0.0625	2650	2.4	1E-3	0.09	0.7
(5) 0.03125	2650	0.62	1E-3	0.06	0.7

The model grids were time stepped with 180, 30, and 15 s (for USE, NYB, and SHF grids) for the ocean, and 300, 60, and 30 s for the wave model. During the few days of landfall simulation, the ocean time steps

were reduced to 45, 15, and 5 s because the ocean currents became considerably stronger and the explicit time stepping stability criteria limited the time steps.

In order to assess the impact of different physical processes, several numerical simulations were performed. Run 1 was a realization that included full exchanges between the ocean and wave models, as described previously. Run 2 was the same as Run 1, but did not allow the effects of waves on currents, and did not impose any surface winds or atmospheric pressure changes on the ocean, but was still forced with tides, baroclinicity, and Coriolis force. Differences between Run 1 and Run 2 will identify the increase of oceanic water levels (surge) due to the storm winds and atmospheric pressure. Results are presented both from each grid separately and as a composite. Because the two-way nested results of the finer grid are averaged back into the coarse grid, the solutions is really seamless with varying spatial resolution. Here we sometimes identify which grid the results are from for clarity.

4. Results

4.1. Water levels

In addition to the effect of tides, changes in water levels along the inner continental shelf and coast occur due to wind-driven flows, Stokes transport, and the lower atmospheric pressure. As the storm tracked north, water levels increased along the entire US East Coast, typically for at least 8 tidal cycles over the storm event. Increased surge occurred along the storm track itself, but predominately to the west and north of the track, with the greatest impact in the NYB. Fig. 5 shows time series of water levels from five locations along the coast (identified in Fig. 1) that were observed (blue lines), and predicted from Run 1 (full storm dynamics, red lines) and Run 2 (reduced forcing on ocean, black lines). At Charleston, SC, there was a slight increase in water levels with a high tide that reached approximately 1.2 m above mean sea level (MSL) near October 28 at 1200 UTC. This was only a surge of approximately 0.40 m greater than a tide that would have occurred without the storm. Further north at Lewes, DE, the maximum water level reached approximately 1.9 m above MSL near October 29 at 1200 UTC, which was a greater surge of approximately 1.2 m over the normal tide level. Peaks in water level at Sandy Hook, NJ, the Battery, NY, and Woods Hole, MA, all occurred near the storm landfall on October 30, 0000 UTC, with maximum water levels of nearly 3.2 m above MSL at Sandy Hook and the Battery, and 1.7 m above MSL at Woods Hole, consistent with observations. These water levels were all greater than the tide-only scenario, with maximum modeled storm surge on the order of 2.6 m at Sandy Hook and the Battery, and 1.3 m at Woods Hole.

The maximum predicted surge for the entire US East Coast and Gulf of Mexico was computed by taking the difference in water of the full simulation with all the forcings (Run 1) minus the simulation with mainly tidal forcing (Run 2). This allows visualization of the distribution of the maximum surge that occurred during the storm (Fig. 1). Along the hurricane track in the open ocean, the surge was on the order of 0.75 m. This is consistent with a change in water level height due to a drop of pressure from about 1025 mb of typical atmospheric pressure to ~945 mb in the eye of the hurricane. This change in pressure resulted in an increase of sea level that can be

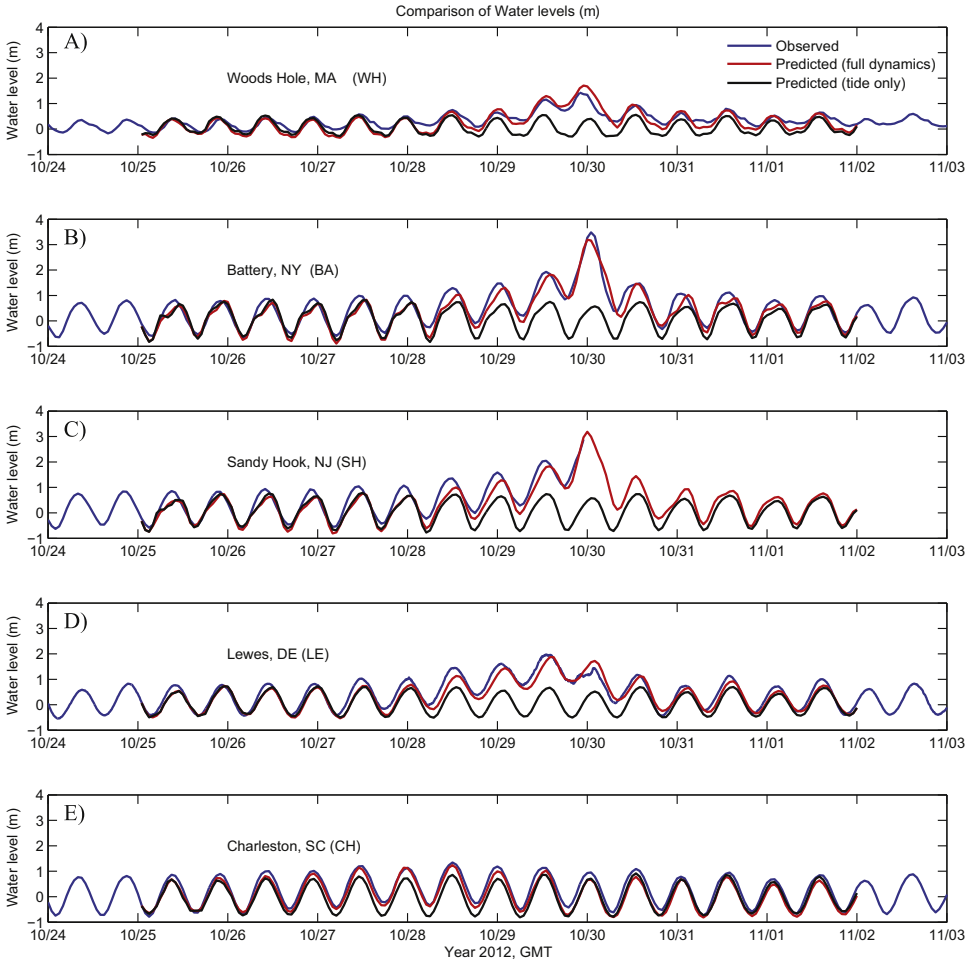

Fig. 5. Time series of water levels (m; MSL) at 5 locations along US East Coast showing observed data (blue), predicted full storm dynamics (red Run 1), and predicted tide only (black Run 2). Locations are shown on Fig. 1A. (For interpretation of the references to color in this figure legend, the reader is referred to the web version of this article)

computed from the hydrostatic balance of $\Delta h = \Delta P/(\rho\ g) = (1025 - 945\ mb)/(1025\ Pa * 9.81\ ms^{-2}) \sim 0.80$ m, where h is water level difference, P is pressure, ρ is density, and g is gravitational acceleration. Along the SAB coastline, the maximum surge was also on the order of 0.70 m that extended across the shelf width (100 m isobath, dotted line on Fig. 1). In the MAB the surge was the greatest in NY Bight region, reaching over 2.5 m. This location was in the right front quadrant of the storm and the shape of the coastline allowed water to be funneled into this region and the water elevation amplified. In Massachusetts Bay, surge also reached over 1 m along the US East Coast due to the wind field extending almost 1000 miles wide just prior to landfall (Schubert et al., 2015). Increased water levels were shown to extend as far north as the Bay of Fundy.

The timing of the maximum surge (Fig. 1B) is consistent with the translation of the hurricane center. Maximum surge occurred along the SAB coast near October 28 (Fig. 1B). At that time the hurricane eye was southeast of the SAB. Similarly, the maximum surge along the coast of the Outer Banks of NC occurred near October 29 at 1200 UTC when the storm was offshore of Cape Hatteras. The maximum surge in the NYB occurred at landfall on October 29 at 2300 UTC. Along the outer shelf, offshore of the MAB-SAB, there are locations that show maximum surge after landfall, occurring when winds were blowing offshore and during relaxation of the inner shelf setup.

4.2. Waves

Hurricane Sandy produced large waves along the entire US East Coast and in the GoM. Comparisons between observed and modeled significant wave heights (Fig. 6) show a strong agreement, with the storm having a distinctive peak in wave height. At the entrance to the Chesapeake Bay (NDBC 44099; water depth ~18 m) wave heights reached up to 5 m with a peak on October 29 at 0200 UTC. Coastal wave heights increased northward reaching up to 7 m at the Delaware Bay entrance (NDBC 44009; water depth ~30 m), and up to 10 m offshore south of Long Island (NDBC 44065; water depth ~25 m) and south of Block Island (NDBC 44097; water depth ~48 m). These buoys were positioned in the northeast quadrant of the storm where wave heights are amplified due to increased surface ocean stress produced by winds blowing in the direction of storm propagation.

The maximum simulated wave heights that occurred at any instance in time during the Hurricane are shown in Fig. 7A. The storm created increased wave heights along the entire US East Coast, with minimal impact in the Gulf of Mexico. While the Hurricane was offshore in the SAB, regions of increased wave height developed offshore of the shelf break (offshore of the 100 m contour, Fig. 7A) reaching over 13 m. Local peak values occurred because the waves were travelling in opposition to the Gulf Stream and therefore the relative wave speed was reduced and created current-induced shoaling of the waves. Landward of the 100 m isobath, the waves were considerably smaller due to wave energy loss from bottom friction, however, heights still reached up to 5 m along the inner continental shelf. As the storm translates, the maximum waves are typically in the right front quadrant (Fan et al., 2009). During Hurricane Sandy, predicted maximum wave heights did occur in the right front quadrant, especially when the storm turned towards the northwest on October 29 at 0600 UTC. Maximum coastal waves occurred where the storm made landfall on the right front quadrant on October 30 at 0000 UTC, and offshore the wave heights reached upwards of 10 m in a band that stretched 1000 km wide.

Generally along a hurricane storm track, wave height maximums precede passage of the eye of the storm, due to reduction of wind stress in the inner eye and lower relative wind speeds on the back side of the storm. However, model results suggest that for Sandy the maximum heights occurred along the track after the eye had passed (Fig. 7B). This is most likely because the storm had multiple peaks of intensity. On October 25 at 0500 UTC the storm had a low pressure of 955 mb, but then gradually weakened until October 26 at 1800 UTC to 970 mb. After that the storm re-intensified until early on October 29 and reached a secondary minimum of 940 mb (Blake et al., 2013). This cycling of intensity can cause wave heights produced in the rear quadrants of a storm during later periods of higher intensity to exceed those produced in the leading quadrants during earlier periods of lower intensity.

Model results suggest that maximum water level surge (Fig. 1) preceded maximum wave heights (Fig. 7) along the track of Hurricane Sandy. This is because the water level displacement at the eye is predominately driven by the reduction in atmospheric pressure. In general during Sandy the timing of the largest wave heights occurred before the highest water levels on the inner continental shelf of the SAB, on the order of 8–15 h. On the inner continental shelf offshore of the Chesapeake Bay mouth the highest water levels occurred before the maximum wave heights on the order of 8–10 h. At the location of landfall, the highest water levels occurred before the maximum wave heights on the order of just a few hours.

4.3. Surface Currents

Ocean surface currents along the US East Coast are driven primarily by tides and surface wind stress. Surface tidal currents in the SAB and MAB can reach up to 0.5 ms^{-1} and typical wind-driven currents can reach up to 1 ms^{-1} (Sullivan et al., 2006; Armstrong et al., 2011, 2014). Coastal surface currents are continuously derived, maintained, and distributed by the High-Frequency Radar National Network (HFRnet; http://cordc.ucsd.edu/projects/mapping/). Data were obtained for the US East Coast, 6 km resolution, hourly real time vectors data set as a combined source from a distributed network of shore-based high-frequency radar systems (HFRADAR). Data are typically available continuously along the US East Coast from Cape Hatteras north to Cape Cod, out to a distance of approximately 350 km. But as Sandy approached data availability became limited in many areas. Modeled surface (upper most grid cell) currents are compared to the HFRADAR measurements.

During Hurricane Sandy the maximum simulated surface stress exceeded 6 Pa offshore of the MAB coastline. On October 29 at 0000 UTC the hurricane was centered approximately 500 km offshore east of Cape Hatteras (latitude 33.9, longitude −71.0). The wind stress drove an enhanced surface current towards the southwest in the MAB and north into the Gulf of Maine (Fig. 8A). Modeled surface currents (black arrows) show an onshore transport and bifurcation of the currents south of Cape Cod that lead west along the southern coast of Long Island and north into the Gulf of Maine. Winds along the coast were predominately towards the southwest and drove a surface current to the west (south of Long Island) and towards the southwest along the coasts of NJ, DE, MD, VA, and NC. Surface currents from the COAWST model also follow the coast and agree with the HFRADAR observations, both in direction and magnitude, with speeds on the order of 0.5 ms^{-1}. The modeled currents show the Gulf Stream meandering towards the northeast with an eddy near the eastern boundary of Fig. 8A. Also the currents split south of Cape Cod to show flow into the Gulf of Maine that match the HFRADAR observations.

As the Hurricane approached the coastline on October 29 at 1800 UTC, the eye was centered in the MAB near −73 longitude and 38 latitude and wind speeds intensified along the coast (Fig. 8B). Coastal surface winds reached near 20 ms^{-1} and the offshore wind speed maximum was over 40 ms^{-1}. South of Long Island winds were still westerly, but farther south, winds along the coast shifted offshore between Delaware and Cape Hatteras. The coastal surface currents increased to over 2 ms^{-1} along the coast offshore of New Jersey south to North Carolina. The strength and direction of the modeled currents are in agreement with the HFRADAR measurements (Fig. 8).

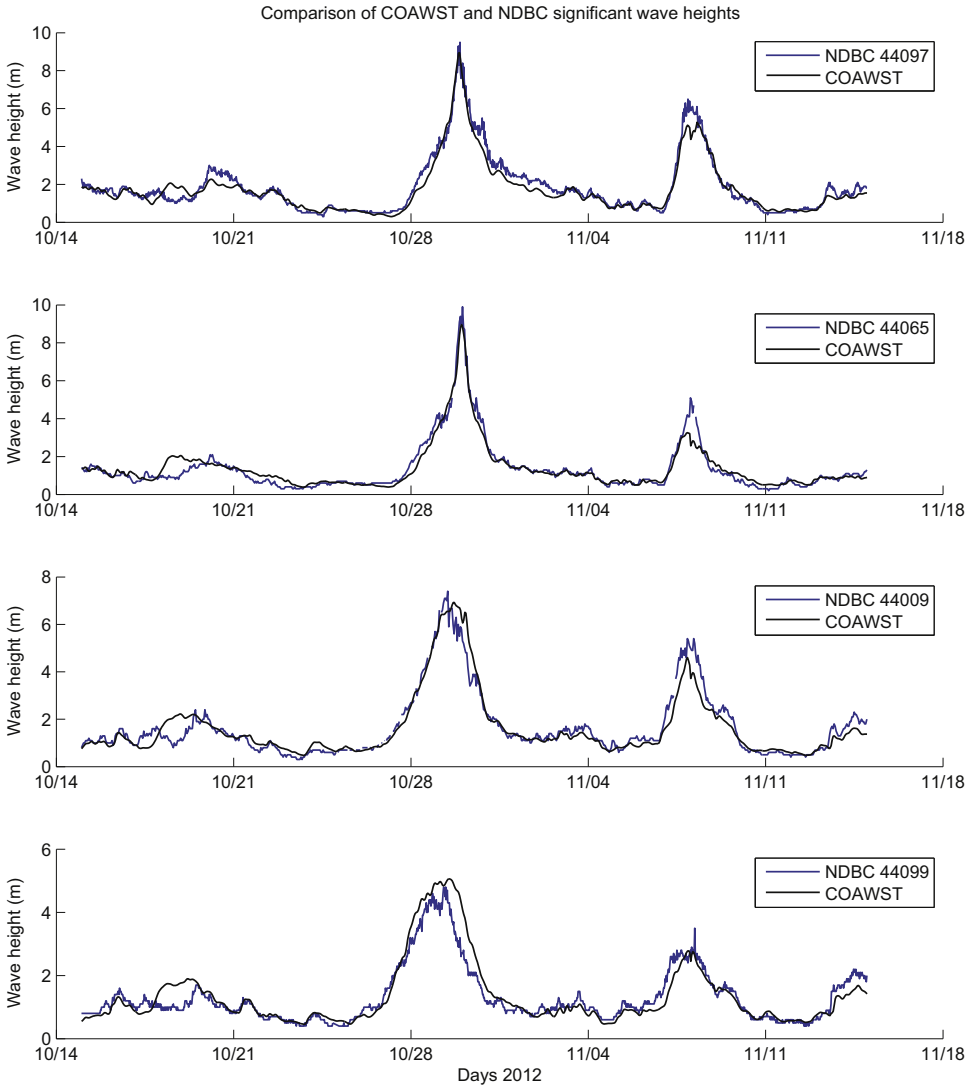

Fig. 6. Time series of significant wave heights at NDBC buoys (positions shown in Fig. 7) for observed (blue lines) and predicted (black lines). (For interpretation of the references to color in this figure legend, the reader is referred to the web version of this article)

4.4. Bottom currents and stress

Modeled bottom (lowest grid cell) currents on the inner continental shelf were typically smaller in magnitude than the surface currents, reaching no higher than 0.5 ms^{-1}. These bottom currents were of sufficient magnitude in combination with waves to produce maximum bottom stress during Hurricane Sandy over 8 Pa (Fig. 9A). In the SAB, bottom stress peaks occurred on the east Florida shelf and across Frying Pan, Cape Lookout, and Diamond Shoals offshore of the Carolinas Capes. In the MAB, bottom stresses were higher and more prevalent over almost the entire continental shelf, with maximums in the right front of the landfall, along the southern edge of Long Island, and offshore of Cape Cod on Nantucket Shoals and Georges Bank.

Focusing on the NYB, the higher-resolution bathymetry in the NYB grid allows for a more detailed representation of the seafloor topography and hence the stresses (Fig. 9B). Along the coast of New Jersey and the southern edge of Long Island the stresses reach as high as ~12 Pa. A zone of reduced stress is evident along the Hudson Shelf Valley, with minimums in the valley resulting from depths exceeding the limits of wave-induced stresses. Further refinement (Fig. 9B) of the SHF grid is overlaid on the NYB grid and shows more detail of stress variation over the SFCRs along southern Long Island. The stresses vary from up to 12 PA at the ridge crests to almost 7 Pa in the troughs. This variation will produce gradients in sediment fluxes causing seafloor changes.

5. Discussion

5.1. Sediment transport

Model results indicated that sediment transport occurred in both bedload and suspended load fractions during Hurricane Sandy. For the simulation, the suspended load was several orders of magnitude larger than the bedload. On the USE grid, the sea-floor sediments were composed of six sediment fractions that were based on the initial distribution from the forecast (Table 1). In the Gulf of Maine (Fig. 10A), the mean bed sediment grain size is coarser over Nantucket Shoals and George's Bank and is on the order of 1 mm, with a finer grain size in the central region of less than 0.1 mm. The net suspended sediment fluxes during the storm show a counter-clockwise rotation in the Gulf of Maine. Flow entered from south of Nova Scotia and traveled northward toward the coast of Maine. A coastal current to the south driven by winds moved sediment southwest along the outer arm of Cape Cod, and south along Nantucket Shoals. Offshore, flux around Georges Bank was clockwise with sediment entering GoM to its west and exiting to its east. The largest sediment flux was westward

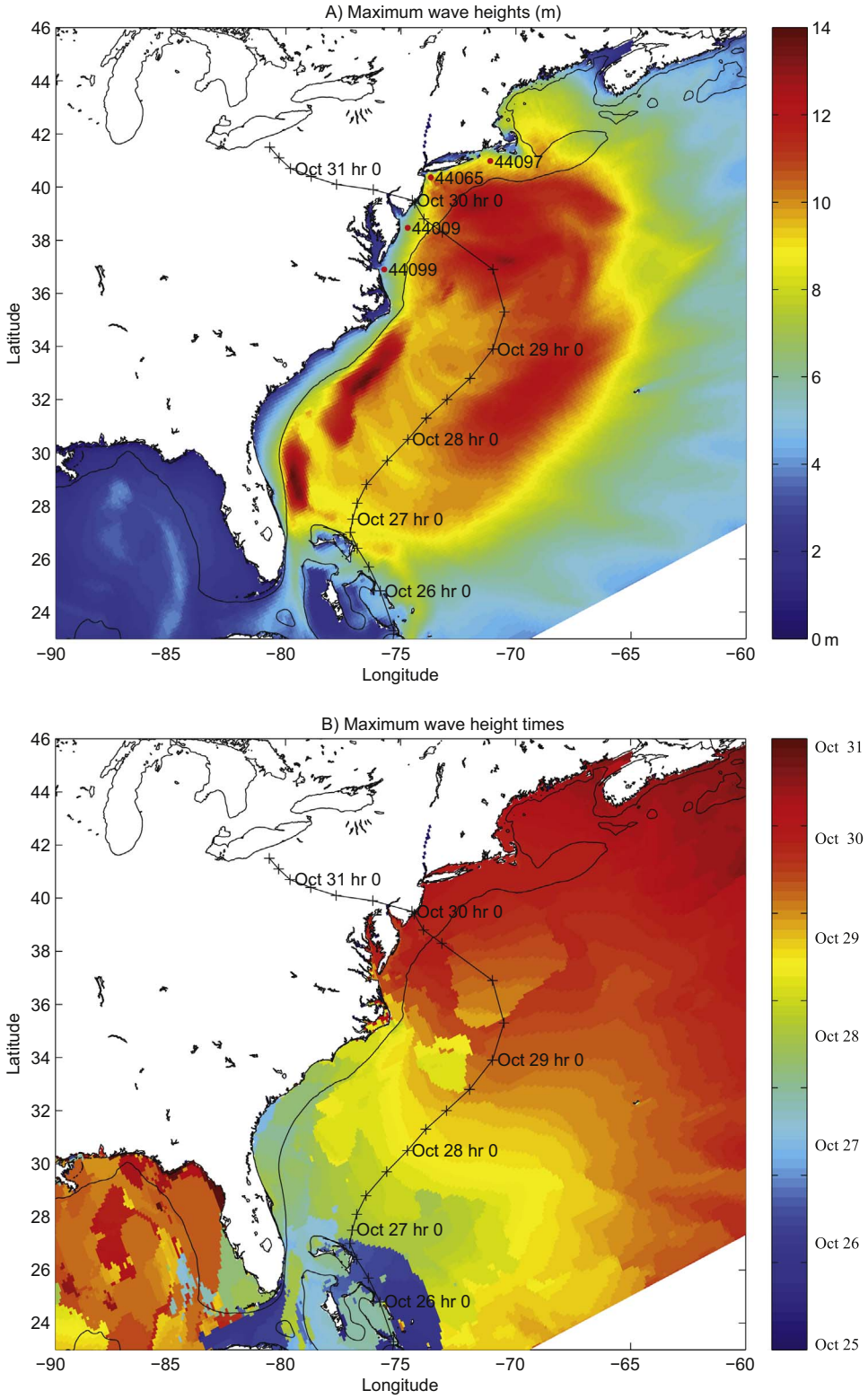

Fig. 7. Map of US East Coast showing track of Hurricane Sandy (black line with -x- and timed positions), 100 m isobaths (thin black line), and numerical results of predicted (A) maximum wave heights and (B) times of maximum waves that occurred during the storm simulation.

south of Cape Cod, where high bottom stresses (Fig. 9) occurred across a relatively shallow region composed of fine-grained, readily erodible sediment.

In the MAB (Fig. 10B) the net suspended sediment flux is to the west and south along the coast. South of Long Island, the sediment is driven west along the coast until it encounters the Hudson Shelf Valley, where the sediment flux is driven southward, down valley and offshore. This net down-valley flux has been observed previously during large storm events (Harris et al., 2003; Lentz et al., 2014). Immediately to the southwest of the valley is a subtle, low relief zone composed of coarser material over which the net flux is slightly offshore and towards the southwest. Along the coast north of the Delaware Bay entrance south to Cape Hatteras the fluxes change in magnitude due to spatial gradients in grain size, and increase towards the Cape as the shelf

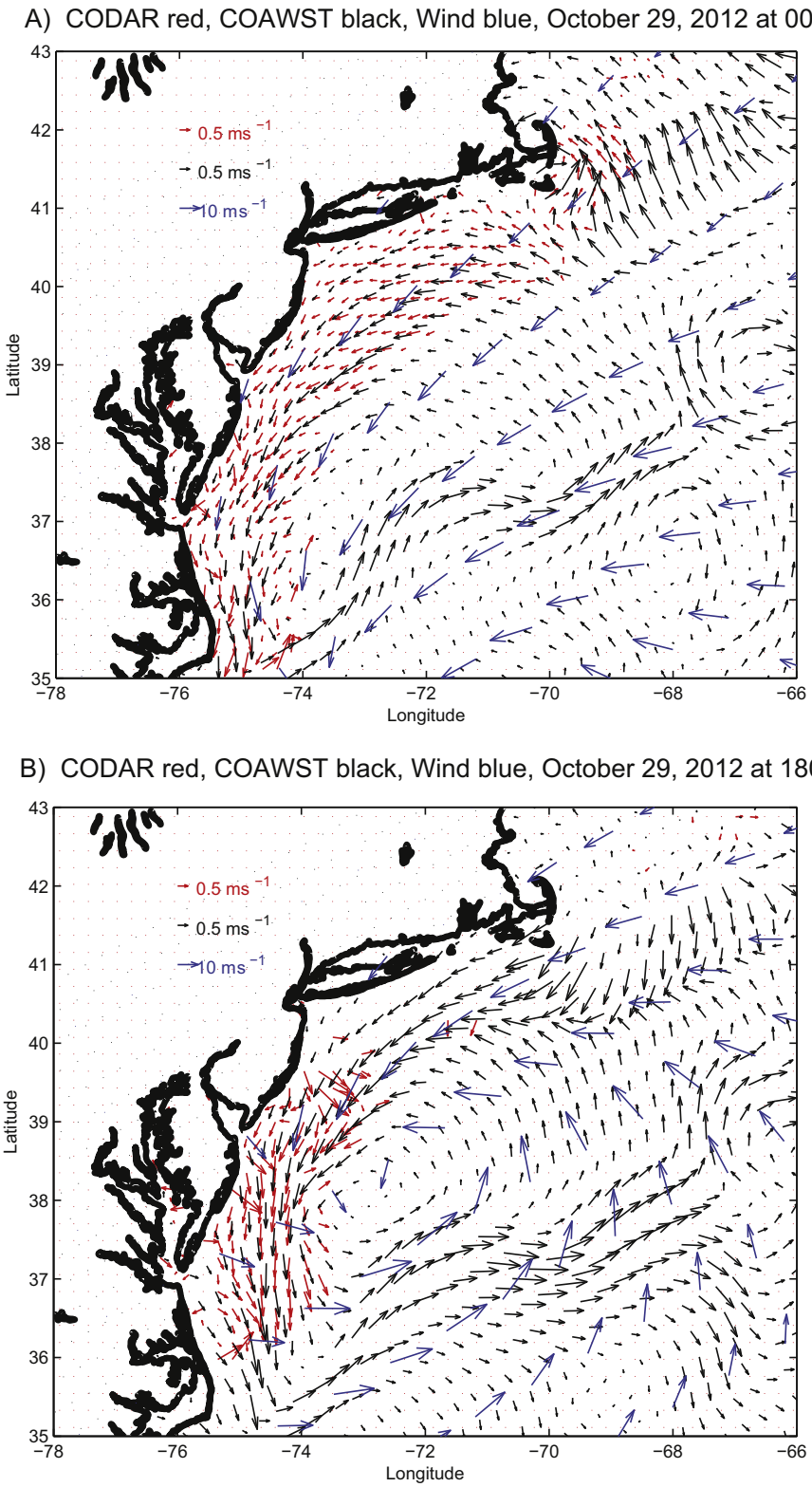

Fig. 8. Comparison of coastal HFRADAR derived surface currents (red) to COAWST surface currents (black), with wind vectors (blue) along US East Coast for Hurricane Sandy at (A) October 29 at 0000 UTC and (B) October 29 at 1800 UTC. (For interpretation of the references to color in this figure legend, the reader is referred to the web version of this article)

narrows and the flows increase.

5.2. Seafloor elevation changes

The predicted gradients in sediment fluxes result in changes to the sediment distribution and seabed elevation. As stated earlier, the magnitudes of modeled seafloor change are dependent on the grain sizes and their properties of erosion rate parameters, settling velocity, and critical stress for mobility. However, sensitivity tests identified that although the magnitudes have uncertainty, the spatial patterns of change remain consistent. These predicted changes in bed thickness vary along the coast, but typically range from +/−0.4 m (Fig. 11A). At

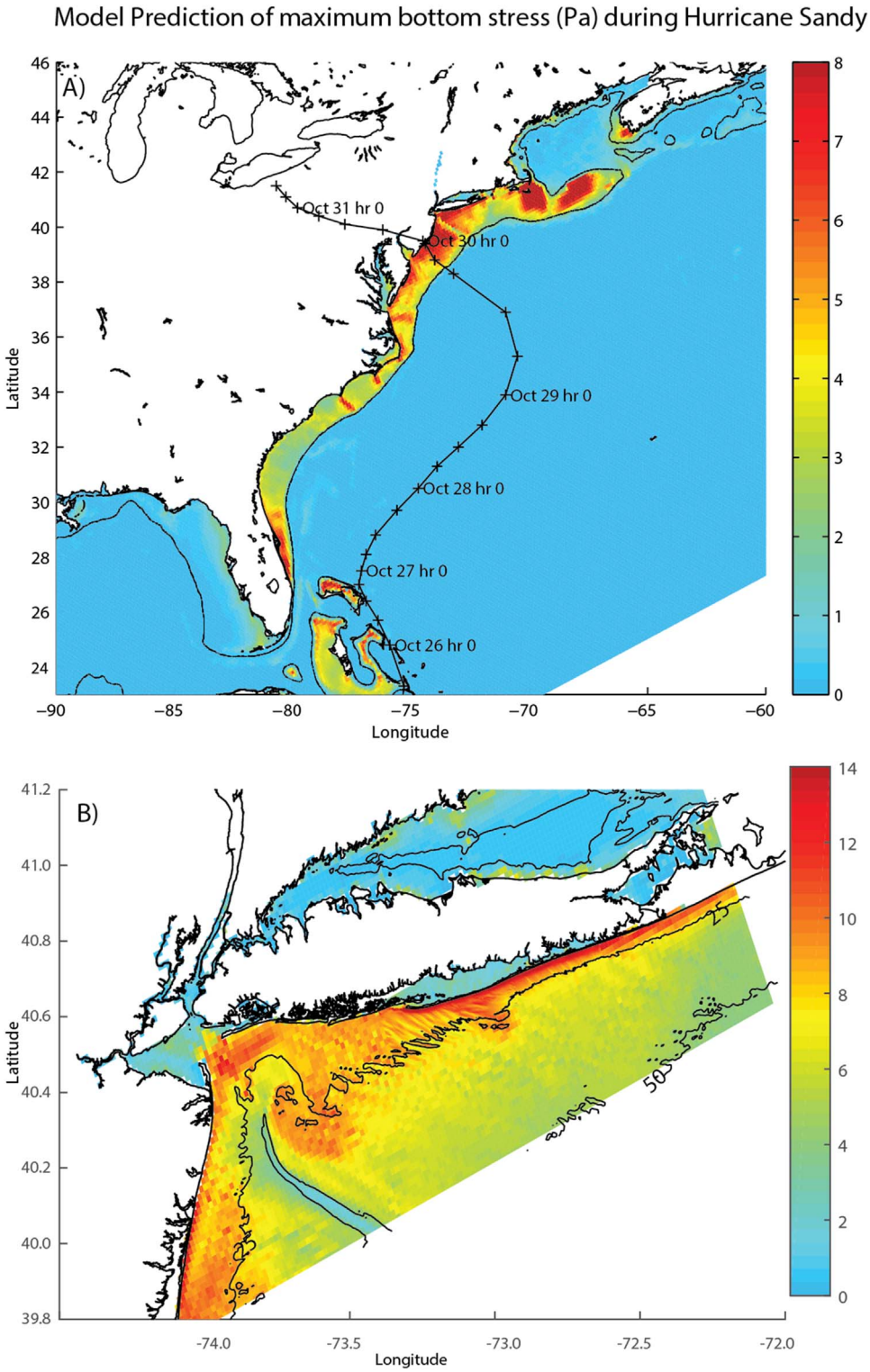

Fig. 9. Maximum combined bottom stress during Hurricane Sandy for (A) USE grid and (B) NYB and SHF (thin outline) grids. Wider range scale in (B) reflects higher resolution of predictions simulated using NYB and SHF grids.

the scale of the USE model grid (5 km grid spacing), the resolved seafloor variations are at the same scale or greater. This means that features such as the width of the inner continental shelf are well simulated. As a finer grid resolves more seafloor features, predicted changes over those features are, in turn, better resolved. In the Gulf of Maine, sediment eroded at the southern tip of Nova Scotia was transported and deposited approximately 25 km to the north. Similar erosion was predicted south of Penobscot Bay, with that material transported southwest and deposited along the coast. One of the larger regions of predicted change is south of Cape Cod, at a location that has a smaller grain size, where erosion on the order of 0.30 m resulted in significant transport and deposition to the west.

In the MAB, alternating patterns of erosion and accretion were predicted along the shelf (Fig. 11A.) Deposition was indicated within the Hudson Shelf Valley, while erosion occurred across its flanks. At Cape Hatteras, intense erosion on the narrow inner-continental shelf

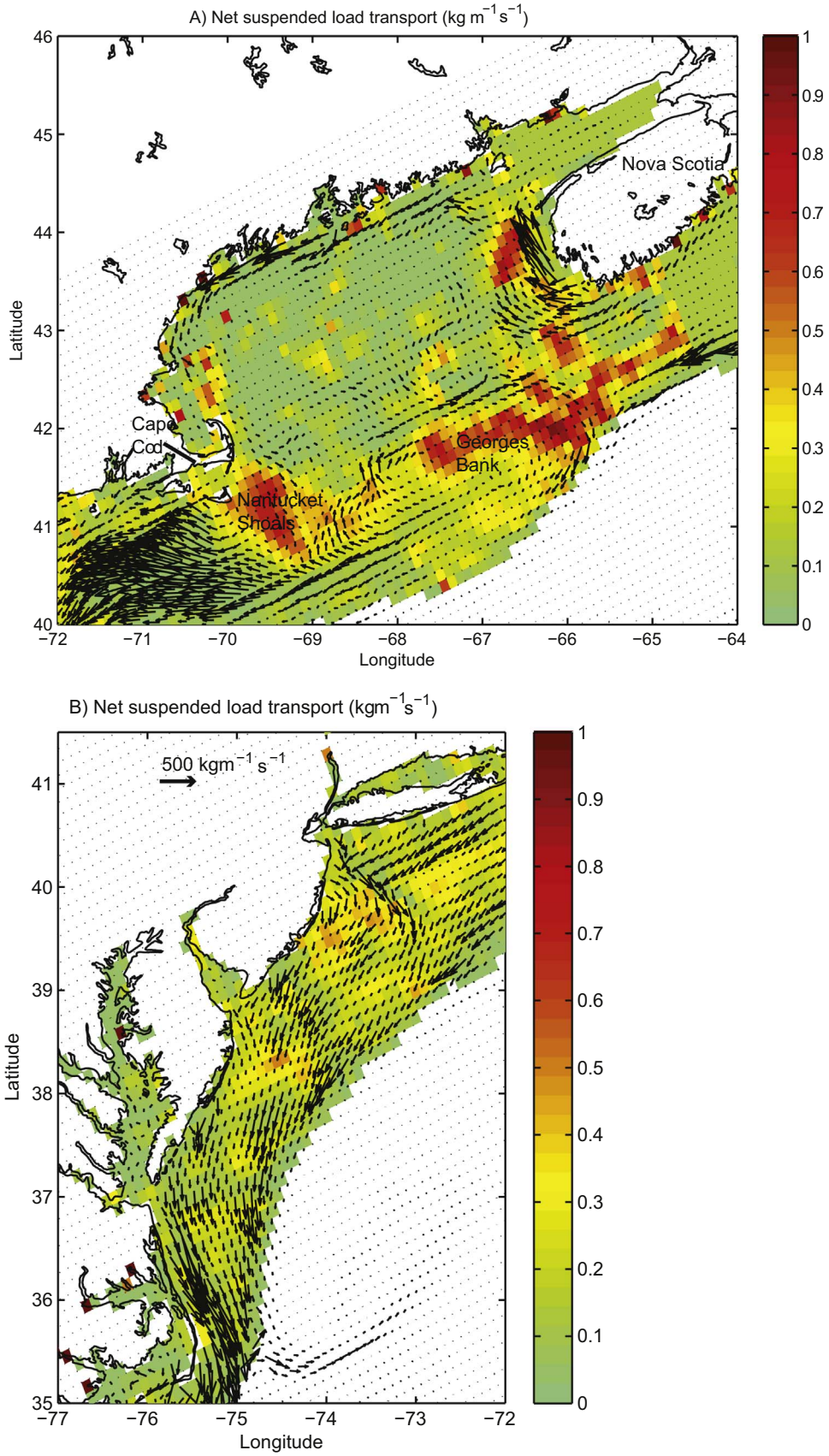

Fig. 10. Color image of mean bottom grain diameter (mm) with arrows showing net suspended-sediment fluxes for A) Gulf of Maine, and B) Mid Atlantic Bight. (For interpretation of the references to color in this figure legend, the reader is referred to the web version of this article)

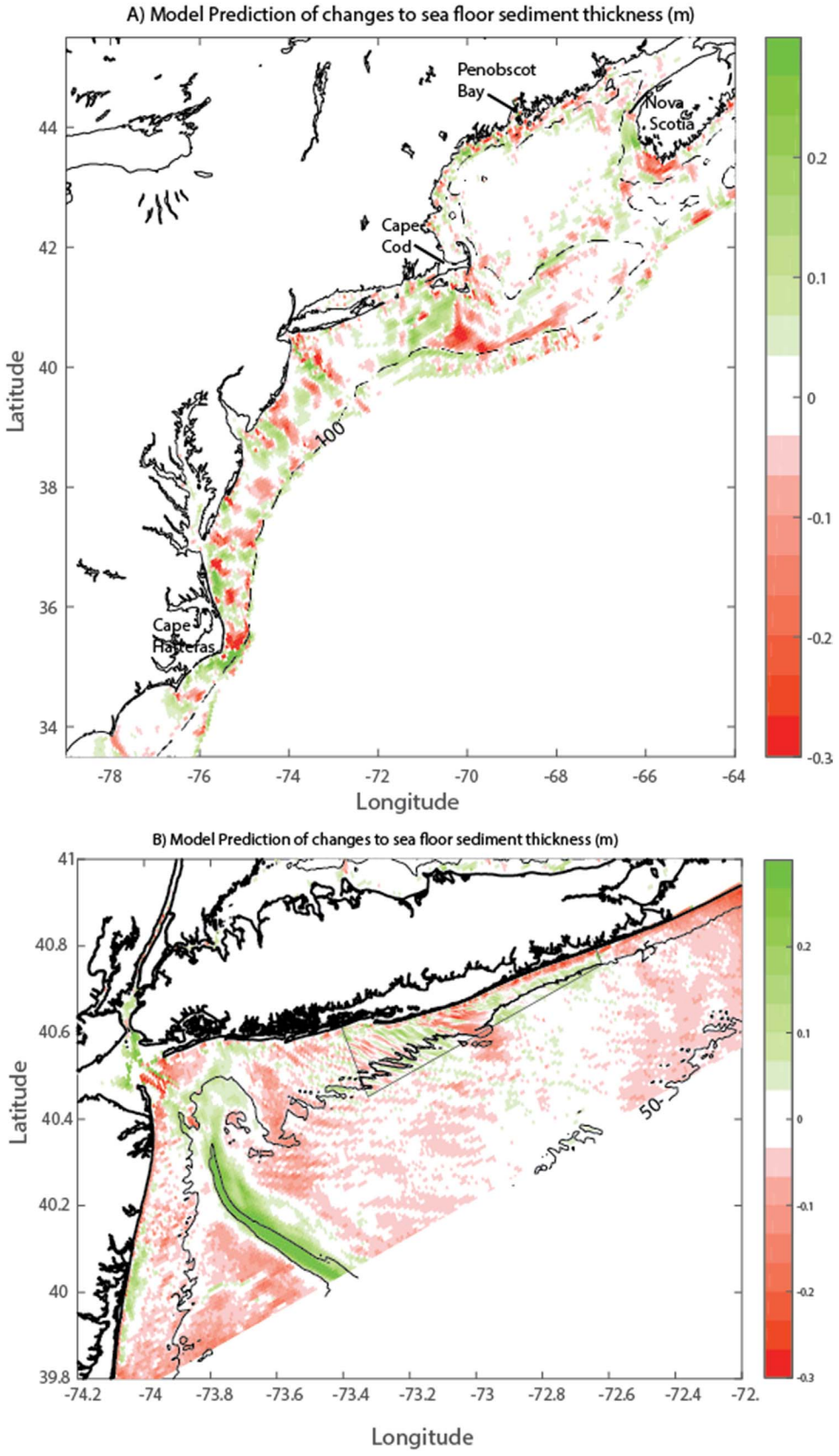

Fig. 11. Changes to seafloor sediment thickness for A) USE (5 km) grid and B) NYB (700 m) grid. Panel (A) uses an evolved initial sediment distribution and panel (B) was initialized uniformly. Results are consistent with deposition in the Hudson Shelf Valley and erosion on the flanks. Change magnitudes < 0.001 m not shown in (A) for clarity.

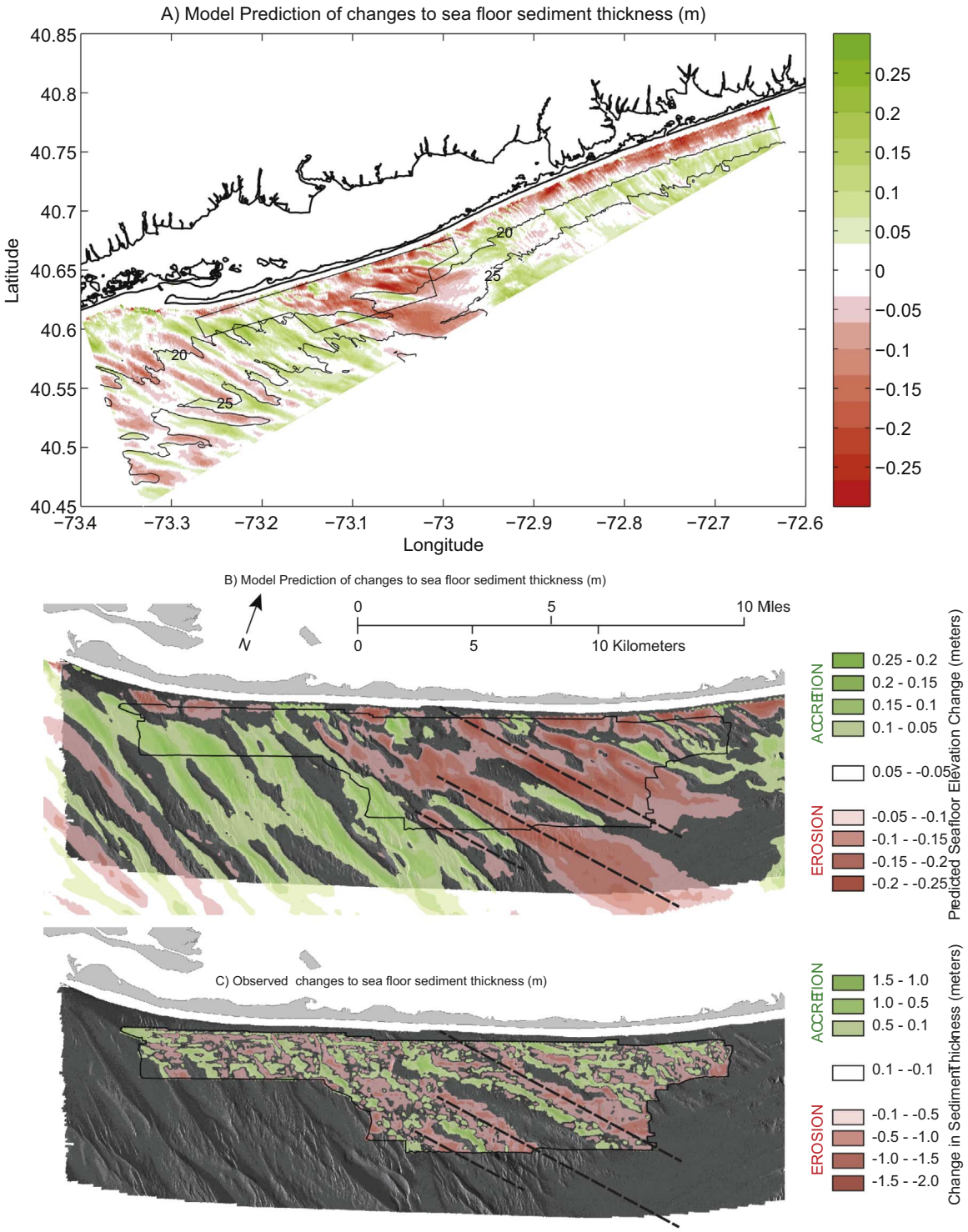

Fig. 12. Comparison of change in modern sediment thickness change for (A) model results along entire length of offshore of Fire Island during Hurricane Sandy; (B) rotated model results along western Fire Island; and (C) measured from seismic-reflection data [2011–2014]. Dashed lines in (B) and (C) show correlated features.

was accompanied by deposition offshore of Diamond Shoals. These patterns in the MAB are very similar to those simulated by Miles et al. (2015), their Figure 14, M2015). Although the spatial patterns are similar, there is a difference in the magnitudes of change in terms of erosion and deposition between M2015 and ours. M2015 Figure 14 shows changes on the order of +/−4 cm, while our Fig. 11 is the best comparison to their work and demonstrates changes on the order of +/−20 cm, which is about 5 times greater, with a few isolated locations with differences up to a factor of 10. This difference is most likely due to several factors including our use of a higher erosion rate, which were based on local observations, and our inclusion of 6 different sediment classes that can create more mobility (mostly from the finest class). There is a need to have more confidence in erosion and deposition calculations based on more observations of the inner shelf seafloor. In the SAB, the major changes were predicted at Cape Lookout and Cape Fear, where sediments were eroded from the shoal crests and deposited to the southwest.

Higher-resolution predictions generated using the NYB grid (Fig. 11B), suggest a region of erosion offshore of central Fire Island (corresponding to the submerged headland), as well as alternating

patterns of erosion and accretion in the vicinity of the SFCRs, and other areas of alternating erosion and accretion patterns along the NJ and Long Island coasts. These results also suggest at least 25 cm of deposition in the along the axis of the Hudson Shelf Valley, consistent with previous findings that suggest down valley driven by westward winds (Lentz et al., 2014).

Numerical results from the SHF grid provide the highest-resolution prediction of seafloor changes along Fire Island (Fig. 12A). Model results show erosion dominated near the coast of eastern Fire Island, with that material being transported to the west and slightly offshore during this event. Modeled results along the eastern region also show alternating zones of erosion and accretion (Fig. 12A), and these linear accretionary zones that extend seaward and are coincident with inner shelf sorted bedforms (Fig. 2). Offshore of the center of the island near the grid boundary is the modeled region of greatest erosion (Fig. 12A) that is consistent with the location of maximum bottom stress. This location is coincident with the high-backscatter gravel area associated with the eroded remains of a buried Pleistocene headland (Fig. 2). It is unknown what actual stresses are needed to liberate sediment from this location. However, the region is overlain with a veneer of sediment that was certainly available to be eroded from this location. Along the central and western segments of the island, in the area of the SFCRs, alternate patterns of erosion and accretion were indicated with erosion on ridge crests and deposition on the lee flanks. The mean change of modeled bed elevation for the region in the grid that is coincident with the geologic mapping (Fig. 12 A, black outlined area) is −0.03 m.

The isopachs of surficial sediment thickness interpreted from the seismic-reflection surveys in 2011 and 2014 are useful for evaluating the sea-floor elevation changes predicted by the model along Fire Island. The difference between the 2011 and 2014 isopach values was computed to yield a 50 m/pixel difference grid that illustrates areal patterns of accretion and erosion over the three-year period within the area common to the two surveys (Schwab et al., 2016; Fig. 12C). In the vertical, a conservative estimate of the vertical resolution limits of the subbottom profiling system is used and differences less than 0.10 m (−0.10 to 0.10 m) are removed when showing change in sediment thickness.

The spatial patterns of modeled bed elevation change on the SHF grid closely agree with the change in modern sediment thickness mapped from the 2011 and 2014 seismic-reflection data (Fig. 12B and C). The isopach difference grid indicates a general pattern consisting of erosion on the northeast-facing ridge flanks and crests of the sand ridges, and deposition on their southwest ridge flanks and in the troughs between them, indicating a net southwesterly migration of the shoreface-connected sand ridges. Statistics computed on the difference grid suggest that the modern sediment volume across the ~81 km^2 of common seafloor mapped in both surveys decreased by 2.8×10^6 m^3; a mean change in sediment thickness of −0.03 m. Results from the model are similar in pattern, but smaller in magnitude. This may be due to the observed difference being from a 3-yr-long time period, but the model difference is from only simulating one large storm event with assumptions of modeled erosion rate parameters and spatial variations in grain size. Direct observations of seafloor sediment changes are difficult to make due to the fact that the changes can be on the order of the accuracy of the measurements at large regional scales. Repeated observations at regional scales are even more difficult.

Thus, the combined impacts of Hurricanes Irene (Aug 2011) and Sandy (Oct 2012) appear to have caused a southwesterly movement of the sand ridges, with sediment eroded from the ridge crests and deposited on the western flanks or troughs. The modeling scenarios simulated for this research focused on Hurricane Sandy, however the impacts of Hurricane Irene are also inherently in the geophysical data comparisons. However, analysis of the COAWST forecast modeling archive show that the modeled impacts of Irene were significantly less than that of Hurricane Sandy, and identifies that Hurricane Sandy was likely to be the dominant impact during this time period.

6. Conclusions

Hurricane Sandy was a severe storm that impacted the US East Coast in October 2012, causing massive coastal impacts. Post-storm assessments identified subaerial changes to the coastal region. To identify subaqueous impacts, geophysical surveys from 2011 and 2014 over coincident areas on the inner-continental shelf offshore of Fire Island, NY, were used to determine modern sediment thicknesses and changes to the seafloor from the storm. Numerical simulations were performed for Hurricane Sandy using a coupled numerical modeling system with grid refinement to resolve increasing spatial resolutions along the US East Coast (5 km), New York Bight (700 m), and offshore of Fire Island, NY (100 m). Comparison of model to observations of water levels, waves, and currents demonstrates skill of the model results and identifies peak locations and times of maximum water levels, wave heights, and bottom stresses. Analysis of the simulated sediment changes shows alternating patterns of erosion and accretion along the east coast, deposition in the Hudson Shelf Valley, and erosion along crests and deposition in the troughs of SFCR offshore of Fire Island. Model results are consistent with the spatial patterns and volumetric magnitudes of surficial sediment changes measured from time series seismic-reflection surveys. Model forecast archived results support the conclusion that the majority of seafloor changes observed are related to the impact from Hurricane Sandy with minor effects from Hurricane Irene.

Acknowledgements

This research was funded by the U.S. Geological Survey (USGS), Coastal and Marine Geology Program, and conducted by the Coastal Change Processes Project. This research was supported in part by the Department of the Interior Hurricane Sandy Recovery program. We acknowledge and appreciate the contributions by USGS and anonymous reviewers. This research used resources provided by the Core Science Analytics, Synthesis, & Libraries (CSASL) Advanced Research Computing (ARC) group at the USGS. Time-series data can be accessed at the USGS Oceanographic Time-Series Database at http://stellwagen.er.usgs.gov/. Model metadata and output can be accessed at the USGS Coastal and Marine Geology Program data portal http://cmgdata.usgsportals.net/#.

References

Armstrong, B.N., Warner, J.C., Voulgaris, G., List, J.H., Thieler, E.R., Martini, M.M., and Montgomery, E.T., 2011. Carolinas coastal change processes project data report for observations near diamond shoals, NC from January–April 2009. U.S. Geological Survey Open-File Report 2011–1156, ⟨http://pubs.usgs.gov/of/2011/1156/⟩.

Armstrong, B.N., Warner, J.C., List, J.H., Martini, M.M., Montgomery, E., Voulgaris, G., and Traykovski, P., 2014. Coastal change processes project data report for observations near Fire Island, New York, January to April 2012. U.S. Geological Survey Open-File Report 2014-1159, ⟨http://pubs.usgs.gov/of/2014/1159⟩.

Bender, M.A., Ginis, I., Tuleya, R., Thomas, B., Marchok, T., 2007. The operational GFDL Coupled Hurricane–Ocean Prediction System and a summary of its performance. Mon. Weather Rev. 135, 3965–3989. http://dx.doi.org/10.1175/2007MWR2032.1.

Blake, E.S., Kimberlain, T.B., Berg, R.J., Cangialosi J.P., Beven II, J.L., 2013. Tropical cyclone report Hurricane Sandy (AL182012) 22–29 October 2012, National Hurricane Center, ⟨http://www.nhc.noaa.gov/data/tcr/AL182012_Sandy.pdf⟩.

Booij, N., Ris, R.C., Holthuijsen, L.H., 1999. A third-generation wave model for coastal regions. Part I: Model description and validation. J. Geophys. Res. 104 (C4), 7649–7666.

Buxton, H.T., Andersen, M.E., Focazio, M.J., Haines, J.W., Hainly, R.A., Hippe, D.J., Sugarbaker, L.J., 2013. Meeting the science needs of the Nation in the wake of Hurricane Sandy – A U.S. geological survey science plan for support of restoration and recovery. U.S. Geological Survey Circular 1390, pp. 26, ⟨http://pubs.usgs.gov/circ/1390/⟩.

Calvete, D., Falqués, A., de Swart, H.E., Walgreen, M., 2001. Modeling the formation of shoreface-connected sand ridges on storm-dominated inner shelves. J. Fluid Mech. 441, 169–193.

Carniel, S., Warner, J.C., Chiggiato, J., Sclavo, M., 2009. Investigating the impact of surface wave breaking on modelling the trajectories of drifters in the Northern Adriatic Sea during a wind-storm event. Ocean Model. 30, 225–239.

Chen, S.Y.S., Price, J.F., Zhao, W., Donelan, M.A., Walsh, E.J., 2007. The CBLAST-

hurricane program and the next-generation fully coupled atmosphere-wave-ocean. Models for hurricane research and prediction. Bull. Am. Meteor. Soc. 88, 311–317.
Craig, P.D., Banner, M.L., 1994. Modeling wave-enhanced turbulence in the ocean surface layer. J. Phys. Oceanogr. 24, 2546–2559.
Denny, J.F., Schwab, W.C., Baldwin, W.E., Barnhardt, W.A., Gayes, P.T., Morton, R.A., Warner, J.C., Driscoll, N.W., Voulgaris, G., 2013. Holocene sediment distribution on the inner continental shelf of northeastern South Carolina: implications for the regional sediment budget and long-term shoreline response. Cont. Shelf Res. 56, 56–70.
De Vet, P.L.M., Stive, M.J.F., Den Bieman, J.P., McCall, R.T., Talmon, A.M., Visser, P.J., Yuan, J., 2014. Modelling Sediment Transport and Morphology During Overwash and Breaching Events (Master Thesis). Civil Engineering and Geosciences, Hydraulic Engineering Department, Delft University of Technology.
Duane, D.B., Field, M.E., Meisburger, E.P., Swift, D.J.P., Williams, S.J., 1972. Linear shoals on the Atlantic inner shelf, Florida to Long Island. In: Swift, D.J.P., Duane, D.B., Pilkey, O.H. (Eds.), Shelf Sediment Transport. Dowden, Hutchinson, and Ross, 447–449.
Falques, A., Calvete, D., de Swart, H.E., Dodd, N., 1998. Morphodynamics of shoreface-connected ridges. In: Proceedings ICCE Copenhagen, Copenhagen, Denmark, 3, June 22–26, 1998, pp. 2851–2864.
Fan, Y., Ginis, I., Hara, T., 2009. The effect of wind-wave-current interaction on air-sea momentum fluxes and ocean response in tropical cyclones. J. Phys. Oceanogr. 39, 1019–1034. http://dx.doi.org/10.1175/2008JPO4066.1.
Figueiredo, A.G., Swift, D.J.P., Stubblefield, W.L., Clarke, T.L., 1981. Sand ridges on the inner Atlantic shelf of North America: morphometric comparisons with Huthnance stability model. Geo-Mar. Lett. 1, 187–191.
Goerss, J.S., 2006. Prediction of tropical cyclone track forecast error for Hurricanes Katrina, Rita, and Wilma. Preprints. In: Proceedings of the 27th Conference on Hurricanes and Tropical Meteorology, Monterey, CA, Amer Meteor Soc 11A.1.
Goff, J.A., Flood, R.D., Austin, J.A., Schwab, W.C., Christiensen, B., Browne, C.M., Denny, J.F., Baldwin, W.E., 2015. The impact of Hurricane Sandy on the shoreface and inner shelf of Fire Island, New York: large bedform migration but limited erosion. Cont. Shelf Res. 98, 13–25.
Haidvogel, D.B., Arango, H.G., Budgell, W.P., Cornuelle, B.D., Curchitser, E., Di Lorenzo, E., Fennel, K., Geyer, W.R., Hermann, A.J., Lanerolle, L., Levin, J., McWilliams, J.C., Miller, A.J., Moore, A.M., Powell, T.M., Shchepetkin, A.F., Sherwood, C.R., Signell, R.P., Warner, J.C., Wilkin, J., 2008. Ocean forecasting in terrain-following coordinates: formulation and skill assessment of the regional ocean modeling system. J. Comput. Phys. 227, 3595–3624.
Hapke, C.J., Brenner, O., Hehre, R., and Reynolds, B.J., 2013. Coastal change from Hurricane Sandy and the 2012–13 winter storm season – Fire Island, New York. U. S. Geological Survey Open-File Report 2013–1231, pp. 37, ⟨http://pubs.usgs.gov/of/2013/1231/⟩.
Harris, C.K., Butman, B., Traykovski, P., 2003. Winter-time circulation and sediment transport in the Hudson Shelf Valley. Cont. Shelf Res. 23, 801–820.
Kirby, J.T., Chen, T.-M., 1989. Surface waves on vertically sheared flows: approximate dispersion relations. J. Geophys. Res. 94, 1013–1027.
Kumar, N., Voulgaris, G., Warner, J.C., Olabarrieta, M., 2012. Implementation of a vortex force formalism in a coupled modeling system for inner-shelf and surf-zone applications. Ocean Model. 47, 65–95.
Leatherman, S.P., 1985. Geomorphic and stratigraphic analysis of Fire Island. Mar. Geol. 63, 173–195.
Lentz, S.J., Butman, B., Harris, C., 2014. The vertical structure of the circulation and dynamics in Hudson Shelf Valley. J. Geophys. Res. Oceans 119, 3694–3713. http://dx.doi.org/10.1002/2014JC009883.
Madsen, O.S., 1994. Spectral wave-current bottom boundary layer flows. Coastal Engineering 1994. In: Proceedings of the 24th International Conference, Coastal Engineering Research Council/ASCE, pp. 384–398.
Marks, F.D., Shay, L.K., 1998. Landfalling tropical cyclones: forecast problems and associated research opportunities. Bull. Am. Meteor. Soc. 79, 305–323.
McKinney, T.F., Stubblefield, W.L., Swift, D.J.P., 1974. Large-scale current lineations on the central New Jersey shelf: investigations by side-scan sonar. Mar. Geol. 17 (2), 79–102.
Miles, T., Seroka, G., Kohut, J., Schofield, O., Glenn, S., 2015. Glider observations and modeling of sediment transport in Hurricane Sandy. J. Geophys. Res. Oceans 120, 1771–1791. http://dx.doi.org/10.1002/2014JC010474.
Miselis, J.L., McNinch, J.E., 2006. Calculating shoreline erosion potential using nearshore stratigraphy and sediment volume: Outer Banks, North Carolina. J. Geophys. Res. 111, 1–15.
Nnafie, A., de Swart, H.E., Calvete, D., Garnier, R., 2014. Modeling the response of shoreface-connected sand ridges to sand extraction on an inner shelf. Ocean Dyn. 64, 723–740. http://dx.doi.org/10.1007/s10236-014-0714-9.
Nelson, J., He, R., Warner, J.C., Bane, J., 2014. Air-sea interactions during strong winter extratropical storms. Ocean Dyn. 64, 1233–1246. http://dx.doi.org/10.1007/s10236-014-0745-2.
Olabarrieta, M., Warner, J.C., Kumar, N., 2011. Wave-current interaction in Willapa Bay. J. Geophys. Res. Oceans 116, C12014. http://dx.doi.org/10.1029/2011JC007387.
Olabarrieta, M., Warner, J.C., Armstrong, B., 2012. Ocean-atmosphere dynamics during Hurricane Ida and nor'Ida: an atmosphere-ocean-wave coupled modeling system application. Ocean Model. 43–44, 112–137.
Peng, S.Q., Liu, D.L., Sun, Z.B., Li, Y.N., 2012. Recent advances in regional air-sea coupled models. Sci. China (Earth Sci.) 55 (9), 1391–1405 http://earth.scichina.com:8080/sciDe/EN/Y2012/V55/I9/1391.
Poppe, L.J., McMullen, K.Y., Williams, S.J., and Paskevich, V.F., (Eds.), 2014. USGS east-coast sediment analysis: Procedures, database, and GIS data (ver. 3.0, November 2014). U.S. Geological Survey Open-File Report 2005-1001, ⟨http://pubs.usgs.gov/of/2005/1001/⟩; ⟨http://coastalmap.marine.usgs.gov/FlexWeb/national/usseabed/⟩.
Renault, L., Chiggiato, J., Warner, J.C., Gomez, M., Vizoso, G., Tintoré1, J., 2012. Coupled Atmosphere-Ocean-Wave simulations of a storm event over the Gulf of Lion and Balearic Sea. J. Geophys. Res., Oceans 117, C09019. http://dx.doi.org/10.1029/2012JC007924.
Riggs, S.R., Cleary, W.J., Snyder, S.W., 1995. Influence on inherited geologic framework on barrier shoreface morphology and dynamics. Mar. Geol. 126, 213–234.
Rogers, R., Aberson, S., Black, M., Black, P., Cione, J., Dodge, P., Gamache, J., Kaplan, J., Powell, M., Dunion, J., Uhlhorn, E., Shay, N., Surgi, N., 2006. The intensity forecasting experiment: a NOAA multiyear field program for improving tropical cyclone intensity forecasts. Bull. Am. Meteor. Soc. 87, 1523–1537.
Schubert, C.E., Busciolano, R., Hearn, P.P., Jr., Rahav, A.N., Behrens, R., Finkelstein, J. S., Monti, J., Jr., Simonson, A.E., 2015. Analysis of storm-tide impacts from Hurricane Sandy in New York. U.S. Geological Survey Scientific Investigations Report 2015–5036, pp. 75, ⟨http://dx.doi.org/10.3133/sir20155036⟩.
Schwab, W.C., Baldwin, W.E., and Denny, J.F., 2016. Assessing the impact of Hurricanes Irene and Sandy on the morphology and modern sediment thickness on the inner continental shelf offshore of Fire Island, New York. U.S. Geological Survey Open-File Report 2015–1238, pp. 15, ⟨http://dx.doi.org/10.3133/ofr20151238⟩.
Schwab, W.C., Baldwin, W.E., and Denny, J.F., 2014a. Maps showing the change in modern sediment thickness on the inner continental shelf offshore of Fire Island, New York, between 1996–97 and 2011. U.S. Geological Survey Open-File Report 2014–1238, ⟨http://dx.doi.org/10.3133/ofr20141238⟩.
Schwab, W.C., Baldwin, W.E., Denny, J.F., Hapke, C.J., Gayes, P.T., List, J.H., Warner, J.C., 2014b. Modification of the quaternary stratigraphic framework of the inner-continental shelf by Holocene marine transgression – an example offshore of Fire Island, New York. Mar. Geol. 355, 346–360.
Schwab, W.C., Baldwin, W.E., Hapke, C.J., Lentz, E.E., Gayes, P.T., Denny, J.F., List, J.H., Warner, J.C., 2013. Geologic evidence for onshore sediment transport from the inner-continental shelf: Fire Island, New York. J. Coast. Res. 26, 536–544.
Schwab, W.C., Thieler, E.R., Allen, J.R., Foster, D.S., Swift, B.A., Denny, J.F., 2000a. Influence of inner-continental shelf geologic framework on the evolution and behavior of the barrier-island system between Fire Island Inlet and Shinnecock Inlet, Long Island, New York. J. Coast. Res. 16, 408–422.
Schwab, W.C., Thieler, E.R., Denny, J.F., Danforth, W.W. Hill, J.C., 2000b. Seafloor sediment distribution off Southern Long Island. USGS Open File Report 00-243, New York.
Shchepetkin, A.F., McWilliams, J.C., 2005. The Regional Oceanic Modeling System: A split-explicit, free-surface, topography-following coordinate oceanic model. Ocean Model. 9, 347–404. http://dx.doi.org/10.1016/j.ocemod.2004.08.002.
Shchepetkin, A.F., McWilliams, J.C., 2009. Correction and commentary for "Ocean forecasting in terrain-following coordinates: formulation and skill assessment of the regional ocean modeling system". by Haidvogel et al., J. Comp. Phys. 227, pp. 3595–3624. Journal of Computational Physics, 228, pp. 8985–9000.
Sopkin, K.L., Stockdon, H.F., Doran, K.S., Plant, N.G., Morgan, K.L.M., Guy, K.K., Smith, K.E.L., 2014. Hurricane sandy – observations and analysis of coastal change. U.S. Geological Survey Open-File Report 2014-1088, pp. 54, ⟨http://dx.doi.org/10.3133/ofr20141088⟩.
Stone, B.D., Borns, H.W., 1986. Pleistocene glacial and interglacial stratigraphy of New England, Long Island, and adjacent Georges Bank and Gulf of Maine. In: Sibraba, V., Bowen, D.Q., Richmond, G.M. (Eds.), Quaternary Glaciations in the Northern Hemisphere. Pergamon Press, Oxford, 38–52.
Stubblefield, W.L., McGrail, D.W., Kersey, D.G., 1984. Recognition of transgressive and post-transgressive sand ridges on the New Jersey continental shelf. In: Tillman, R.W., Siemers, C.T. (Eds.), Siliclastic Shelf Sediments 34. SEPM Special Publication, 1–23.
Sullivan, C.M., Warner, J.C., Martini, M.A., Voulgaris, G., Work, P.A., Haas, K.A., Hanes, D.H., 2006. South carolina coastal erosion study data report for observations. October 2003–April 2004, U.S. Geological Survey Open-File Report 2005-1429. ⟨http://pubs.usgs.gov/of/2005/1429/⟩.
Swift, D.J.P., Field, M.E., 1981. Evolution of a classic sand ridge field: Maryland sector North American inner shelf. Sedimentology 28, 461–482.
Swift, D.J.P., Freeland, G.L., 1978. Current lineations and sand waves on the inner shelf, middle Atlantic Bight of North America. J. Sediment. Petrol. 48, 1257–1266.
Taylor, P.K., Yelland, M.J., 2001. The dependence of sea surface roughness on the height and steepness of the waves. J. Phys. Oceanogr. 31, 572–590.
Teague, W.J., Jarosz, E., Wang, D.W., Mitchell, D.A., 2007. Observed oceanic response over the upper continental slope and outer shelf during Hurricane Ivan. J. Phys. Oceanogr. 37, 2181–2206.
Trowbridge, J.H., 1995. A mechanism for the formation and maintenance of shore-oblique sand-ridges on storm-dominated shelves. J. Geophys. Res. 100, 16,071–16,086.
Uchiyama, Y., McWilliams, J.C., Shchepetkin, A.F., 2010. Wave–current interaction in an oceanic circulation model with a vortex-force formalism: application to the surf zone. Ocean Model. 34, 16–35. http://dx.doi.org/10.1016/j.ocemod.2010.04.002.
Wada, A., Kohno, N., Kawai, Y., 2010. Impact of wave-ocean interaction on Typhoon Hai-Tang in 2005. Sci. Online Lett. Atmos. 6A, 13–16.
Wang, Y., Wu, C.C., 2004. Current understanding of tropical cyclone structure and intensity changes - a review. Meteor. Atmos. Phys. 87, 257–278. http://dx.doi.org/10.1007/s00703-003-0055-6.
Warner, J.C., Sherwood, C.R., Signell, R.P., Harris, C., Arango, H.G., 2008. Development of a three-dimensional, regional, coupled wave, current, and sediment-transport model. Comput. Geosci. 34, 1284–1306.
Warner, J.C., Armstrong, B., He, R., Zambon, J., 2010. Development of a Coupled Ocean-Atmosphere-Wave-Sediment Transport (COAWST) Modeling System. Ocean Model.

35, 230–244 http://woodshole.er.usgs.gov/project-pages/cccp/public/COAWST.htm.
Warner, J.C., List, J., Schwab, B., Voulgaris, G., Armstrong, B.A., Marshall, N., 2014. Inner-shelf circulation and sediment dynamics on a series of shore-face connected ridges offshore of Fire Island, NY. Ocean Dyn. 64, 1767–1781. http://dx.doi.org/10.1007/s10236-014-0781-y.
Wren, P.A., Leonard, L.A., 2005. Sediment transport on the mid-continental shelf in Onslow Bay, North Carolina during Hurricane Isabel. Estuar., Coast., Shelf Sci. 63, 43–56.
Zambon, J.B., He, R., Warner, J.C., 2014a. Investigation of Hurricane Ivan using the Coupled Ocean-Atmosphere-Wave-Sediment Transport (COAWST) Model. Ocean Dyn. 64, 1535–1554. http://dx.doi.org/10.1007/s10236-014-0777-7.
Zambon, J.B., He, R., Warner, J.C., 2014b. b, Tropical to extratropical: marine environmental changes associated with Superstorm sandy prior to its landfall. Geophys. Res. Lett., 41. http://dx.doi.org/10.1002/2014GL061357.